EPA-600/2-76-144
May 1976

Environmental Protection Technology Series

ELECTROSTATIC PRECIPITATORS: RELATIONSHIP BETWEEN RESISTIVITY, PARTICLE SIZE, AND SPARKOVER

Industrial Environmental Research Laboratory
Office of Research and Development
U.S. Environmental Protection Agency
Research Triangle Park, North Carolina 27711

RESEARCH REPORTING SERIES

Research reports of the Office of Research and Development, U.S. Environmental Protection Agency, have been grouped into five series. These five broad categories were established to facilitate further development and application of environmental technology. Elimination of traditional grouping was consciously planned to foster technology transfer and a maximum interface in related fields. The five series are:

1. Environmental Health Effects Research
2. Environmental Protection Technology
3. Ecological Research
4. Environmental Monitoring
5. Socioeconomic Environmental Studies

This report has been assigned to the ENVIRONMENTAL PROTECTION TECHNOLOGY series. This series describes research performed to develop and demonstrate instrumentation, equipment, and methodology to repair or prevent environmental degradation from point and non-point sources of pollution. This work provides the new or improved technology required for the control and treatment of pollution sources to meet environmental quality standards.

EPA REVIEW NOTICE

This report has been reviewed by the U.S. Environmental Protection Agency, and approved for publication. Approval does not signify that the contents necessarily reflect the views and policy of the Agency, nor does mention of trade names or commercial products constitute endorsement or recommendation for use.

This document is available to the public through the National Technical Information Service, Springfield, Virginia 22161.

EPA-600/2-76-144
May 1976

ELECTROSTATIC PRECIPITATORS: RELATIONSHIP BETWEEN RESISTIVITY, PARTICLE SIZE, AND SPARKOVER

by

Herbert W. Spencer, III

Southern Research Institute
2000 Ninth Avenue South
Birmingham, Alabama 35205

Contract No. 68-02-1303
ROAP No. 21ADL-027
Program Element No. 1AB012

EPA Project Officer: Leslie E. Sparks

Industrial Environmental Research Laboratory
Office of Energy, Minerals, and Industry
Research Triangle Park, NC 27711

Prepared for

U.S. ENVIRONMENTAL PROTECTION AGENCY
Office of Research and Development
Washington, DC 20460

ABSTRACT

The report gives results of a study of the relationships of the electrical resistivity of fly ash, its particle size, the occurrence of back corona and sparkover, and the electrical characteristics of electrostatic precipitators (ESP's). The study included laboratory measurement of the dielectric strengths and resistivity of five particle-size fractions of a fly ash sample and measurement of the current densities and voltages at which back corona and sparkover occurred for a 3-mm dust layer covering the plate of a wire-plate negative-corona discharge device. Results showed that the peak current density for the formation of back corona depended on the resistivity of the dust covering the positive electrode. Operating current densities for full-scale ESP's are discussed in relation to fly ash resistivity.

CONTENTS

FIGURES

FIGURES
(Cont'd)

TABLES

SECTION I
CONCLUSIONS

The efficiency of an electrostatic precipitator is a direct function of the electrical conditions that are obtained in the precipitator. By increasing the electric field and particulate charge, the migration velocity of the particles to the collection plate can be increased, resulting in increased efficiency or reducing the size of the precipitator needed to meet a given emission standard. Unfortunately, precipitators are forced to operate at voltages and current densities significantly below what can be obtained with a corona discharge system containing no particulate. The resistivity of the particulate collected on the plates of an electrostatic precipitator inversely affects the current density at which the precipitator can operate.

Data are presented in this report for full scale precipitators and for a laboratory corona discharge device that show the dependence of precipitator electrical operation on particulate properties. The field data indicate that precipitators collecting particulate with resistivities below $\sim 1 \times 10^{10}$ Ω-cm can operate at current densities on the order of 80 nA/cm^2. At this current density the electric field in the collected dust layer is less than 0.8 kV/cm^2 for particulate with resistivities below 1×10^{10} Ω-cm. This electric field is less than the dielectric strength of the collected particulate, which is usually on the order of 20 kV/cm. Current densities for precipitators collecting particulate with resistivities above 1×10^{10} Ω-cm were observed to decrease with resistivity. However, considerable scatter was obtained in the data. Some units operated at current densities producing electric fields in the collected particulate layer near the dielectric strength of the layer, while others operated at current densities a factor of 10 to 20 times below the limit set by the dielectric strength and resistivity of the dust layer. It is estimated that spatial and temporal variations in current density

can account for a suppression in the operating point a factor of 2 or more below the limit set by the particulate resistivity and dielectric strength.

The peak current densities obtained in the laboratory for the formation of back corona were within approximately 20% of the point at which the dielectric strength of the layer would have been exceeded. Field operating points were expected to be set by the point at which back corona occurs; a comparison of our field and laboratory measurements indicates a discrepancy between field operation and small scale corona discharge operation. For low resistivities, the data indicate that a considerable increase in operating current densities might be obtained with proper design. For high resistivity dust the scatter in the field data was such that a clear interpretation is not possible. However, it appears as mentioned before that the field units operate a factor of 10 to 20 times below the expected operating point.

The comparison of the laboratory and field measurements in this report shows that in the design of precipitators the minimum and maximum clean plate current density limits must be considered. For very high resistivity dust, the minimum clean plate stable operating density must be below the current density for formation of back corona. For low resistivity ashes ($<10^9$ Ω-cm), precipitator electrical design should allow for operating at current densities in the range of 100 nA/cm^2 if maximum performance is to be obtained.

The objective of the laboratory study was to determine if there were other particulate properties besides dust resistivity that affect the operation of a corona discharge when a dust layer is deposited on the collection electrode.

It was determined that the particulate resistivity was the main factor. Other factors such as particle size, bulk density, porosity, cross sectional area of voids, and specific surface area appeared to affect operating points for precipitators only by their effect on the resistivity of the collected dust layer. A measurable change in the dielectric strength of the collected dust layer as a function of the above factors was not observed for the ash samples studied during this work.

It was observed that ash resistivity varied as a function of particle size and that if the ash is sufficiently fractionated by particle size in the precipitator, a decrease in ash resistivity from the inlet to the outlet can occur. The decrease can exceed a factor of 2 and result in a corresponding increase in operating current density from the inlet to the outlet of the precipitator. The operating electrical data tabulated in this report for full scale units show an increase in current density from the inlet to the outlet. The data also showed that lower operating voltages are normally obtained in the outlet sections of the precipitator. Precipitator electrical behavior cannot be entirely explained by dust resistivity alone; the decrease in space charge effects due to suspended dust from the inlet to the outlet are probably responsible for the observed increase in current density for a given voltage.[1] Space charge effects due to particulate should be included in any future laboratory studies. Theoretical calculations of the voltage-current characteristic for a wire-duct configuration that include space charge effects should be developed for interpreting variations in the voltage-current characteristics of full scale units.

A misaligned corona wire was shown to increase the chance for formation of back corona and sparkover. It was observed that by decreasing the wire to plate spacing the ratio of the peak current density to average current density was increased. It was also observed that the peak current density at the formation of back corona is independent of the wire to plate spacing. The result of these two observations is that if a wire is misaligned, back corona will form at an average current density less than the expected value. Misalignment may account for some of the discrepancy between the operating electrical characteristics of field units and laboratory devices. The magnitude of the effect for precipitators would need to be determined with a multi-wire system.

Other factors such as the variations in dust layer thickness and errors in in-situ resistivity measurements may also play a part in the discrepancy between field units and laboratory measurements. An investigation of the in-situ resistivity measurement procedure is needed to determine if the procedure is affecting the results. The variations in dust layer thickness produced by nonuniform rapping probably produce significant variations in current density, increasing the probability of back corona for a given average current density, and should be investigated. The effects on current density distribution could be determined by measuring the current densities to various points on a precipitator plate covered with a non-uniform dust layer. The non-uniform dust layer would be formed by rapping the plate to remove some of the dust, and then precipitating a new dust layer on the surface.

Measurements of the current density distributions for the following conditions: no dust layer, dust layer without back corona, and dust layer with back corona showed a drastic change in current density distribution with the formation of back corona. This had been previously observed by Kercher.[2] Back corona had the

effect of increasing the average current density while leaving the current densities in some places unchanged.

FUTURE RESEARCH

Further investigation will be needed to clearly delineate the difference between full scale units and a small scale corona discharge when a particulate is present. A determination of the exact current density at which a precipitator can operate for a given set of dust properties will depend on further investigations. Such studies are needed if accurate performance characteristics are to be theoretically determined for electrostatic precipitators.

Specific areas for future research are as follows:

1. Gathering of additional data correlating operating points of field units and dust resistivity.
2. Further development of the correlation between laboratory resistivity measurements and in-situ measurements.
3. Test in a dry pilot scale precipitator to study the effect the following factors have on the electrical behavior of electrostatic precipitators:
   a. Design of electrodes (wires and plates)
   b. Dust properties
   c. Uniformity of current density distribution with and without dust layers
   d. Thickness and uniformity of dust layers
   e. Space charge
   f. Gas composition
4. Theoretical calculations of V-I characteristics for a parallel plate precipitator including space charge effects.

SECTION II
INTRODUCTION

The objective of this research is to provide information for interpreting the electrical behavior of electrostatic precipitators when that behavior is governed by the characteristics of the collected dust layer.

Dust layers affect precipitator electrical behavior in several ways. For one, they introduce a resistance element into the electrical circuit, which, except for the nonlinear characteristics of the resistivity of dust layers, behaves in the same manner as the incorporation of an ohmic resistor in the circuit. Second, the electrical breakdown of the dust layer and the resulting formation of point corona in the dust layer, called by the descriptive terms "back corona", "back ionization", "back sprays", and "back discharge", drastically affect the electrical behavior of a precipitator. Back corona occurs when a highly conductive point is formed in the dust layer, usually by electrical breakdown of the dust at a point where the current density is such that the ohmic buildup of voltage exceeds the dielectric strength of the dust. These visible discharges in negative corona affect precipitator operation by decreasing sparkover potential, increasing the average current density, and producing positive ions that neutralize the negative space charge in the corona gap.

The sparking and back corona conditions for fly ash were investigated using a negative corona wire-plate discharge device in the laboratory. In particular, the variation of corona characteristics as a function of the properties of dust layers formed from different particle size fractions of fly ash was studied. The resistivities, dielectric strengths, porosities, mass median diameters, and chemical compositions of 5 particle size fractions of a fly ash were determined.

Different particle size fractions were studied because precipitators fractionate the inlet dust, the particles collected in the inlet sections being larger than those in the outlet sections. Previous attempts to relate sparkover to particle size have not been successful.[3]

SECTION III

HISTORICAL REVIEW OF STUDIES ON THE EFFECTS OF DUST LAYERS ON ELECTRICAL CHARACTERISTICS OF CORONA DISCHARGES

In 1918, Wolcott[4] found that a dielectric sheet of discontinuous surface placed over the plate electrode of a point-plane electrode system lowered the sparkover voltage by about 50% for negative corona, although it affected positive corona only slightly. In 1933, Franck[5] observed that dust layers also influence the characteristics of discharges, especially in an asymmetric electrode arrangement. For a negative corona discharge, he found that the sparking voltage decreased to about 1/3 of that without a dust layer. The sparkover voltages increased with thicker dust layers from a minimum at approximately 1.5 mm, presumably because of the increased potential drop across the dust layer needed to reach breakdown.

Franck interpreted the phenomenon of breakdown in terms of the relative dielectric constants and conductivities of dust and air. The dust layer and air at the dust layer boundary were assumed to be homogeneous dielectrics with homogeneous fields. The ratio of the electric field in the gas (E_1) to the electric field in the dust layer (E_2) is given by

$$\frac{E_1}{E_2} = \frac{\varepsilon_2}{\varepsilon_1}$$

when there is no current and

$$\frac{E_1}{E_2} = \frac{\sigma_2}{\sigma_1}$$

when there is a current, where $\varepsilon_1, \varepsilon_2$ are the dielectric constants and σ_1, σ_2 are the conductivities of the air and the dust layer, respectively. Because the dielectric constant of the dust is greater

than the dielectric constant of air, the electric field in the dust layer is smaller than the electric field in the air above the dust layer when the potential is first applied. At steady state, the electric field in the dust layer is larger than the field in the air above the layer if the conductivity of the layer is low.

When the break-down voltage of the dust layer is reached, thin conductive channels appear as spots in the dust layer. These spots redistribute the field and behave like corona points (back corona). For negative corona, this produces a strong anodic field, lowering the potential for sparkover. For positive corona, a strong anodic field exists prior to the breakdown of the dust, and thus the effect on sparkover is not as great.

In 1948, White[6] ascribed the detrimental effects of back corona in reducing the collection efficiency of an electrostatic precipitator to a lowering of the sparkover potential and to the production of positive ions which decrease the efficiency of charging of suspended dust particles in a negative corona. He noted that the electrical field (E) in the dust is determined by the product of the current density and the dust resistivity, according to Ohm's Law. Therefore, in an electrostatic precipitator collecting a typical dust having a resistivity of 10^{10} Ω-cm and a dielectric strength of 10 kV/cm, back corona would set in at an operating current density of 1 μA/cm^2.

Using voltage pulses of 1-2 microsecond duration, White obtained peak current densities which were far greater than the direct current densities for the formation of back corona. This can be explained in part by the estimated charging time of 30 microseconds for a layer of dust with 10^{11} Ω-cm resistivity. The voltage across the dust layer for a pulsed current is less than the voltage for a direct current when the pulses are shorter than the charging time and when the time between pulses is longer than the discharge time.

In a series of papers, Penney[7-10], reported on the effects of resistivity layers on both the electrodes of corona discharges. The term "flare" was used to denote a discharge consisting of repetitive current pulses or streamers which originate from a fixed location on the anode when the anode is partially covered by a high resistivity material. Penney's experiments showed a reduction in sparkover potential for negative corona with increased resistivity and with decreased wire size. Although not reported, the reduction as a function of wire size was probably related to increased current densities obtained with the smaller wires, for a given potential. By using a negatively charged ball, Penney was able to show that the flares were a source of positive ions. The flares consisted of current pulses of 0.05 μ-sec rise time and 0.5 μ-sec decay times with a period of approximately 0.33 μ-sec between peak current pulses of 30-80 mA. Penney's experiments indicated that with an imperfect insulating coating on the anode and a source of ionization,current pulses followed by sparkover can occur if the average gradient is of the order of 5 kV/cm. This gradient is significantly below the gradient of 30 kV/cm for breakdown of gases between clean metallic electrodes. Penney suggested that the space charges resulting from the flare produce a gradient which is favorable to the development of a spark or at least alter the field, so that the initial voltage distribution is rather unimportant.

An investigation of back corona in high-resistivity dust layers by Kercher[2] showed that there was a slight variation in the current density at which back corona formed for a layer thickness < 3mm but that Ohm's Law held for a thickness > 3mm. He also showed that when back corona formed the discharge current was concentrated at the breakdown sites.

The effect of resistivity on the formation of back corona has also been studied by Simm.[11] He substantiated previous work, but observed that the sharp increase in current with the formation of back corona was at a somewhat higher current density than Ohm's Law predicted. This indicates that back corona may occur before a distinct change in the voltage-current characteristics is visible.

Apparently the effect of particle size of the dust on back corona has not been adequately studied. In experiments with different particle-size fractions of fly ash, Penney[3] found that the larger particle-size fraction he was using had a lower sparkover potential than a smaller particle-size fraction, even though the resistivity of the large particle-size fraction was lower. However, the larger particle-size fraction contained highly conductive carbon particles.

Electrical operating conditions in industrial electrostatic precipitators have been simulated by Herceg[12] using a point-to-plane corona device and layers of porous insulating materials to simulate precipitated dust layers. In this work he attempted to physically model the corona discharge device by a lumped-element circuit based on a systematization of corona phenomena into four regions described as the primary ionization, accumulation, transport, and secondary-ionization regions. A solid-state analog was designed on the basis of the lumped-element circuit model. However, no data were presented with the design to show that it did model a point-to-plane corona discharge.

Hall[13] has indicated that the practical limits of operating current density are calculated from Ohm's Law, in which the breakdown voltage (E) has a value of 1-2 kV/cm, approximately an order of magnitude smaller than the measured dielectric

strengths of dust layers. White[14] has indicated that the precipitation rate parameter of field units (an empirical parameter that characterizes the performance of a given precipitator under a specified set of operating conditions) varies inversely with the resistivity of the dust being collected by the unit. The practical effects of dust layers on precipitation are summed up in graphs by Hall[13] (Figure 1) and by White[14] (Figure 2).

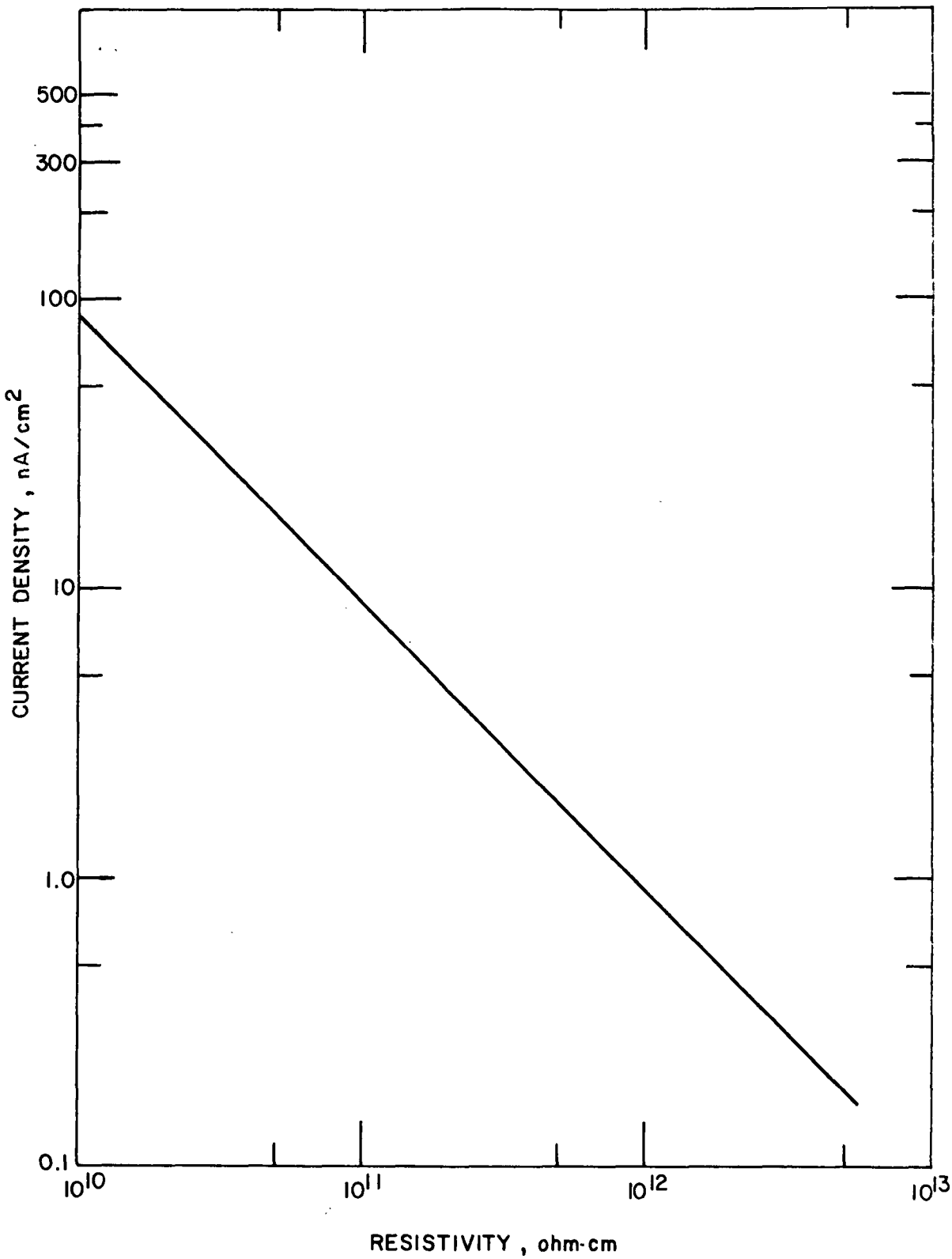

Figure 1. Allowable current density as a function of resistivity according to Hall.[13]

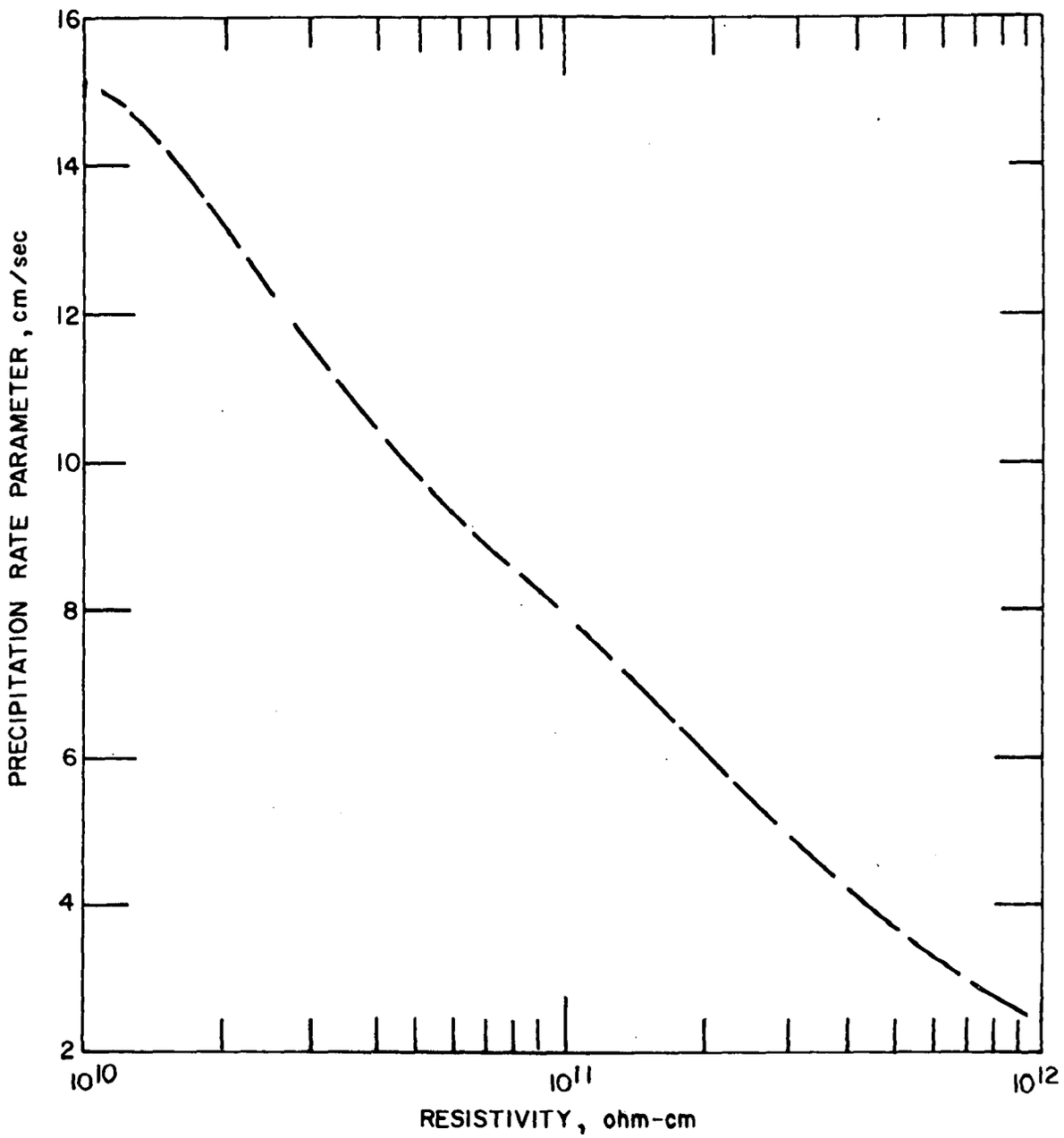

Figure 2. Precipitation rate parameter vs resistivity; Dashed curve White's field data.[14]

SECTION IV
APPARATUS AND PROCEDURES

This section describes the equipment and the procedures used to study the influence of dust layers on the electrical behavior of a wire-plate corona discharge.

CORONA DISCHARGE DEVICE

The wire-plate corona discharge device used in the laboratory experiments is shown schematically in Figures 3 and 4. It consists of a 0.089 cm (0.035 in.)-diameter stainless steel corona wire supported 6.0 cm above a 10-cm square stainless steel plate. The plate electrode is recessed 3 mm in a Teflon block. Five insulated segments are incorporated for measuring the current density at five separate points on the plate.

A Hipotronics DC power supply capable of providing 100 kilovolts maintains high negative potentials on the corona wire of the corona discharge device (ripple is less than 0.5% of output voltage, when operating the device). The corona discharge device is installed in an environmental chamber so that temperature and humidity can be controlled during the measurements. A Teflon-insulated copper tube extending to the device at the bottom of the chamber is connected at the top of the chamber to a voltage divider (a Hipotronics Model 100 high voltage meter). The corona current to any one of the five insulated plate segments or the current to the outer plate is measured by selectively connecting the desired element to the current-measuring circuit displayed in Figure 5 while shorting the other elements of the flat-plate electrode to ground. The current measuring circuit consists of a spark protector, a 100 Ω resistor, and a Keithley 414A picoammeter. The voltage across the 100 Ω resistor in series with the electrometer is amplified five times by a differential amplifier and displayed on a 10 MHz oscilloscope for recognition of back corona onset.

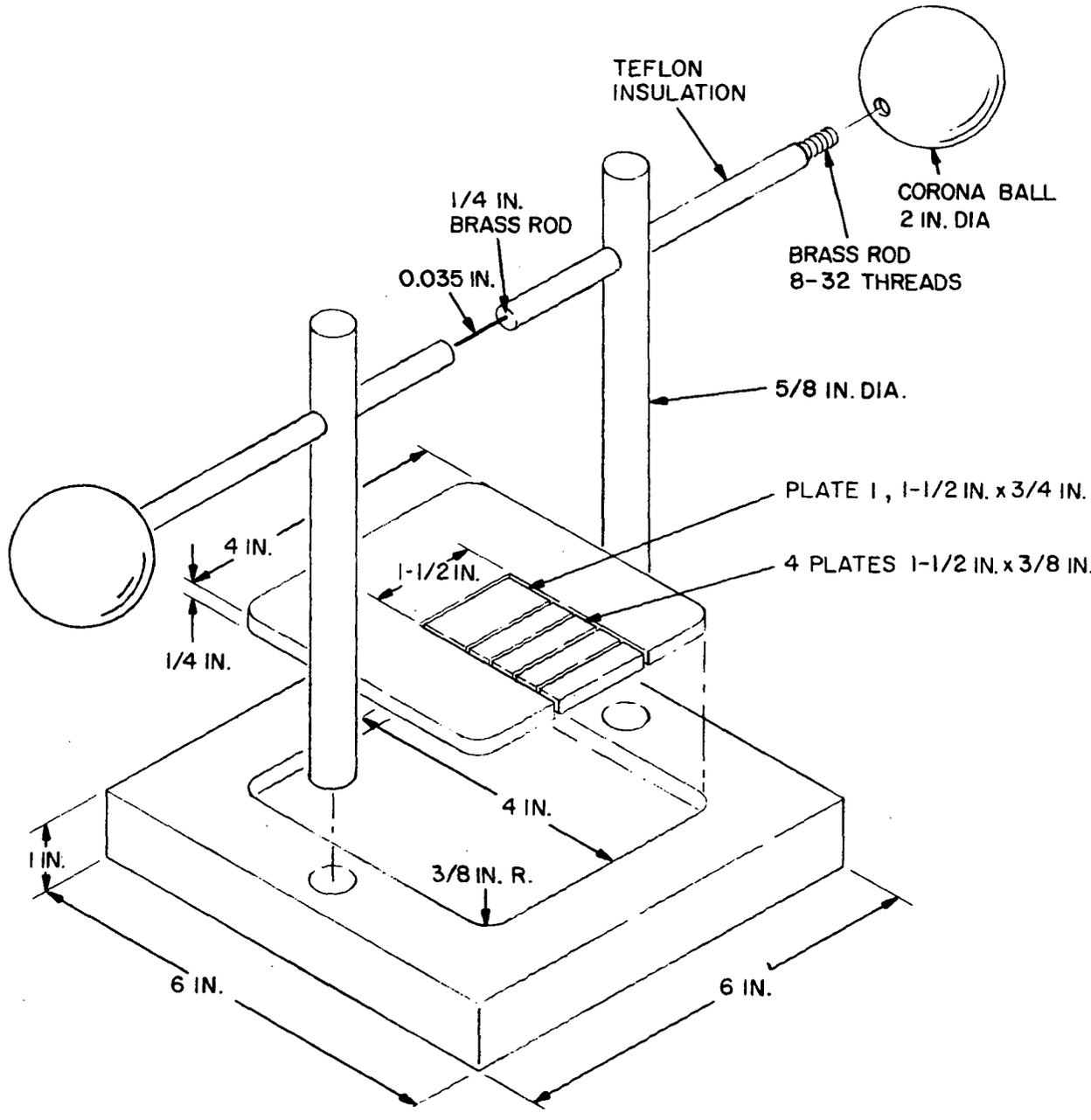

Figure 3. Wire plate corona discharge device

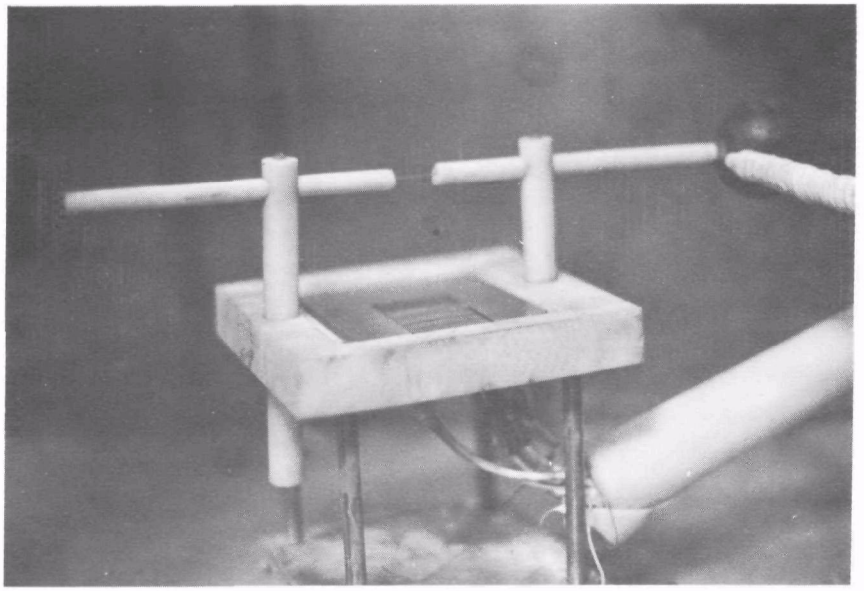

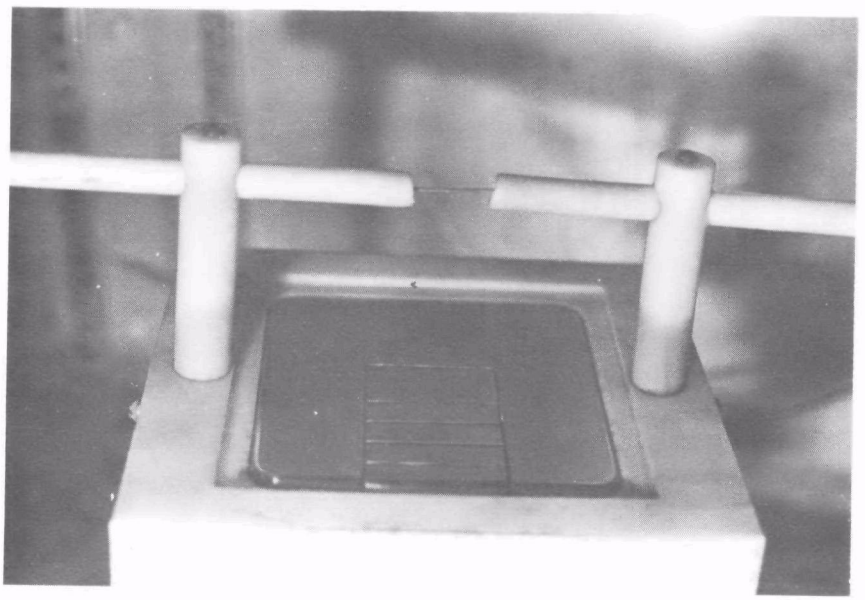

Figure 4. Photographs of the wire plate corona discharge device.

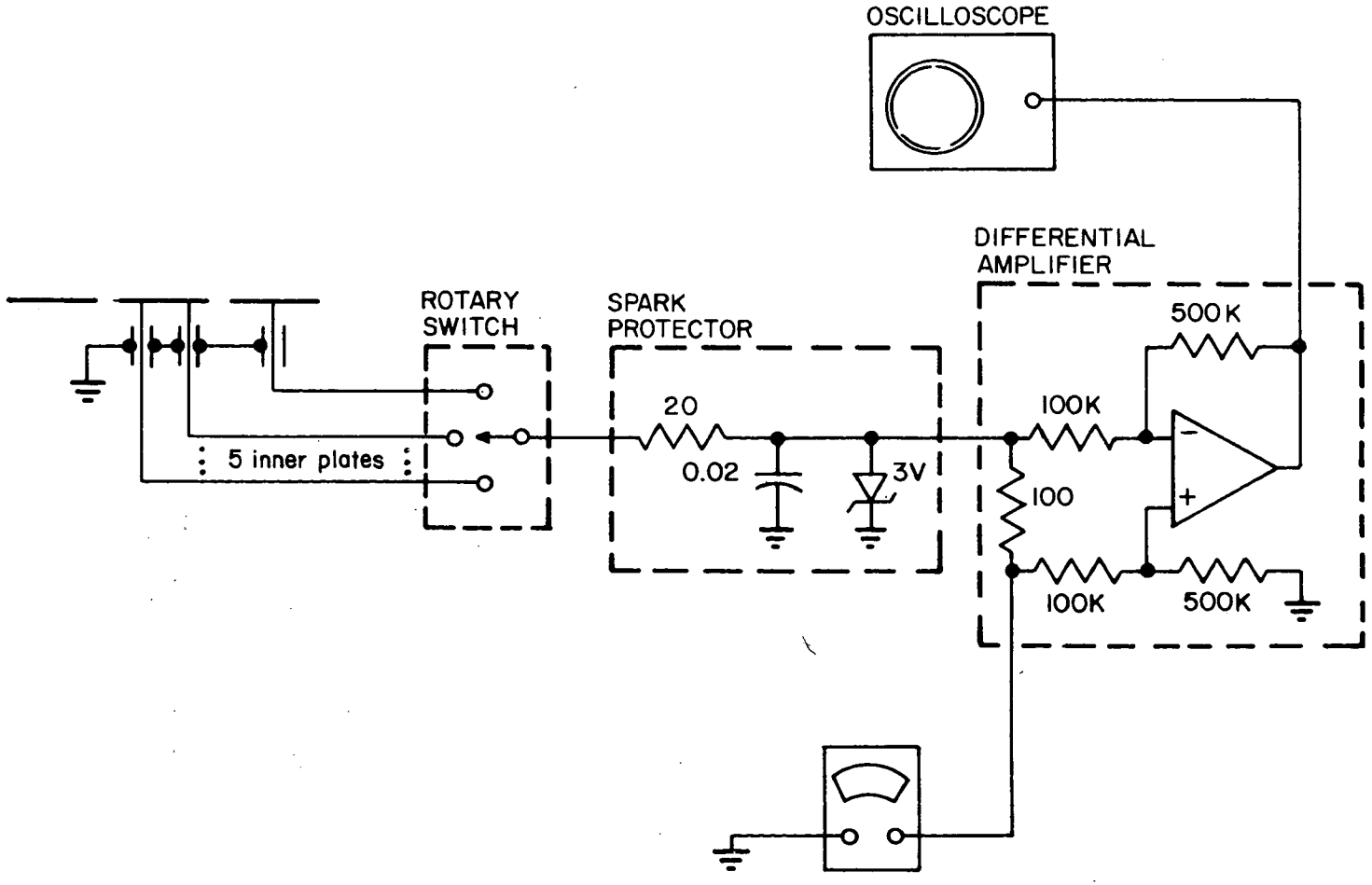

Figure 5. Wire plate corona discharge device circuit schematic

By rounding the edges of the flat collecting plate and by mounting corona balls on the ends of the corona wire support, the maximum clean-plate voltages were increased to above 70 kV and the maximum clean-plate current densities were increased to ~8 $\mu A/cm^2$ (8 mA/ft^2). This current density limit is about a factor of 80 larger than peak current densities in full-scale precipitators.

RESISTIVITY AND ELECTRICAL BREAKDOWN APPARATUS

The electrical resistivity of the fly ash was measured in a conductivity cell built to the specifications of the American Society of Mechanical Engineers Power Test Code 28. The cell consists of an electrode cup for holding the ash sample and a flat electrode with a guard ring that is placed lightly on the dust layer. Voltage is supplied to the electrode by a Keithley 240 A high-voltage supply. The current through the cell is measured with an electrometer assembly similar to that used with the corona discharge device.

Dielectric strength measurements on the fly ash samples were made in a specially designed cell (Figure 6). The cell incorporates a Power Test Code 28 conductivity cell cup for holding the sample and an upper electrode with rounded edges machined from stainless steel. A Peschel Instruments 24-kV high-voltage supply furnishes a negative potential. The overload protection indicator on the power supply is used for detecting breakdown. Dielectric breakdown of air was measured with the same equipment. These pieces of equipment were installed in an environmental chamber so that temperature and humidity could be controlled during the measurements.

ENVIRONMENTAL CHAMBER

Temperature and humidity are controlled and monitored in an insulated chamber housing the wire-plate corona discharge device,

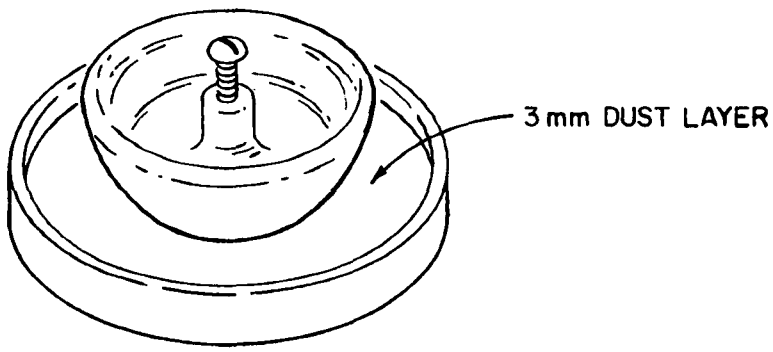

Figure 6. Electrode configuration for testing dielectric strength of ash layer

resistivity cells, and ash and air breakdown cells. System air is bubbled through a temperature-controlled water bath for humidity regulation. This air is heated by two thermostatically-controlled heating elements mounted directly in front of a fan which circulates air through the chamber. Two other heaters, rheostatically controlled, heat the air before it passes through the fan and as it is blown into the chamber. This combination of heaters allows continuous control of temperature to 180°C. The humidity in the chamber is controllable from 1% to 15% water vapor by volume with an approximate accuracy of 1%.

Temperature inside the chamber is monitored by chromel-alumel thermocouples at various locations in the chamber. A 150°C mercury thermometer is visible through a glass window in the chamber.

Moisture content of the chamber atmosphere is determined by weighing the water absorbed by a cylinder of Drierite ($CaSO_4$) after a known volume of air is drawn through the cylinder from the chamber. An Atkins dew point indicator continuously monitors the relative moisture content.

PROCEDURES

Ash from the Gaston Power Station, Wilsonville, Alabama, was separated into five particle-size fractions by the Donaldson Company of Minneapolis, Minnesota. From these size fractions, samples were quartered out and screened through an 80-mesh screen, to break up large agglomerates and to remove any trash present in the sample. Smaller samples were quartered out from the above sample for chemical analysis, resistivity measurements, dielectric strength measurements, and back corona measurements.

The sample for the back corona measurement is placed on the plate of the corona discharge device and is smoothed to a depth of 3 mm while shaking and vibrating the device to compact the

dust layer. The same procedure is used to fill the two resistivity cells and the dielectric breakdown cell.

These devices are then placed in the environmental chamber. The electrodes are put in place on the dust layers and electrical connections are made to each device. A check of electrical connections is made before closing the chamber. After the chamber is closed the temperature and humidity controls are adjusted to give the desired conditions by increasing temperature and moisture from ambient conditions.

Once the environmental conditions are stabilized, electrical readings are made.

The plate current distribution in the corona discharge device is measured as a function of voltage for determining the voltage-current characteristics, back corona, and sparkover data. The voltage is adjusted and read from a Hipotronics Model 100 high voltage meter. At constant voltage, inputs from the plate segments are consecutively switched to a picoammeter and these currents recorded. As current readings are seldom constant, only as many significant figures as indicated by the current range are recorded, or the range of current fluctuation is recorded with the most consistent value of current. Current readings are taken starting at applied voltages of 10 kV and then at applied voltages up to 60-70 kV in increments of 2 to 4 kV. The size of the increment depends on the stability of the voltage-current characteristics.

Oscilloscope waveforms of the current are noted concurrently with the current measurements. Visual observations of the device are also recorded.

The resistivity-cell current measurements are taken one minute after voltage is applied. Current values from both cells are consecutively read at one voltage by switching the picoammeter input from one to the other. The data are taken so that each

cell is read at two applied voltages, 200 V and 1000 V.

Determination of breakdown potentials in dust and air follows an identical procedure. Voltage to the cell is slowly and steadily increased at about 500 V/sec until the supply overload indicator shows sparkover. The potential at that point is recorded.

CALCULATIONS

Current densities for the wire-plate and resistivity cells are calculated as the current divided by the appropriate electrode area. Resistivity, ρ, from the resistivity cell data is calculated by Ohm's Law and the definition of resistivity:

$$\rho = \frac{RA}{D}$$

$$R = \frac{V}{I}$$

so that $$\rho = \frac{V}{I} \cdot \frac{A}{D}$$

where

I = current from cell
V = voltage applied (200 or 1000 V)
R = resistance of ash layer
D = depth of ash layer
A = area of electrode

SECTION V

RESULTS OF LABORATORY MEASUREMENTS

The current-voltage characteristics of the test device were measured with a clean and with a dust-covered plate at various temperatures from 60°C to 180°C and at humidities in the range of one percent to fifteen percent water vapor by volume. Simultaneously, the resistivity and dielectric strengths of the ash layers were measured. Layers of fly ash having mass median diameters of 2.3 μm, 3.6 μm, 8.2 μm, 14.5 μm, and 40 μm were used for the study. Particle size fractions having these mass median diameters were obtained by mechanically separating fly ash from the Gaston Power Station into the following size fractions: 0-3 μm, 3-5 μm, 5-7 μm, 7-15 μm, and >25 μm. The mass median diameter of these particle size fractions were determined by Bahco analysis of each size fraction.

The current density at which back corona forms theoretically depends on the ratio of the dielectric strength and the resistivity of the ash. The dielectric strengths of the different particle size fractions of the Gaston ash are tabulated in Table I. Corresponding values for air are given in this table for a 3 mm gap between electrodes similar to the ones used for the ash electrical breakdown measurements.

The average dielectric strength of the 3 mm dust layers is 22.7 kV/cm, with a standard deviation of 2.3 kV/cm. The average dielectric strength of the 3 mm air gap was 36.9 kV/cm* with a standard deviation of 0.5 kV/cm. The dielectric strengths of the different particle-size fractions bear no definite relation to the particle size. The data also indicate no correlation of the dust dielectric strength with either temperature or resistivity.

---

*According to Paschen's Law for a 0.3 mm gap with a uniform field the dielectric strength of air at p = 720 Torr and T = 293°C is 35.23 kV/cm.[15]

TABLE I

DIELECTRIC STRENGTHS OF ASH LAYERS

Ash Particle Size	T(°C)	H_2O(%)	Ash Breakdown (kV)	Dielectric Strength Ash kV/cm	Resistivity ρ(Ω-cm)	Dielectric Strength Air kV/cm
15-25 µm	60	1.0	6.8	22.7	4.4×10^{10}	36.3
	70	2.0	6.1	20.3	2.9×10^{12}	36.7
	80	1.6	6.6	22.0	1.3×10^{12}	37.3
	100	2.4	6.8	22.8	5.6×10^{12}	37.7
	120	3.0	7.2	24.0	2.0×10^{13}	37.3
	140	3.4	6.5	21.7	5.6×10^{13}	36.5
	160	3.9	8.0	26.8	1.3×10^{13}	36.7
	180	4.7	7.9	26.3	6.4×10^{12}	37.0
0-3 µm	100	3.0	7.3	24.3	2.9×10^{10}	
	160	4.0	7.5	25.0	8.3×10^{11}	
3-7 µm	100	2.7	6.8	22.8	1.2×10^{12}	
	160	4.3	7.3	24.2	2.2×10^{12}	
7-15 µm	100	3.0	5.4	18.0	8.1×10^{11}	
	160	4.0	6.5	21.7	2.0×10^{12}	
>25 µm	100	2.4	6.8	22.8	2.4×10^{12}	
	160	3.6	6.1	20.2	2.6×10^{12}	

Average ash breakdown 6.8 kV

D. C. voltage increased at the rate of 0.5 kV/sec.
Dust layer thickness was 3 mm.

Some investigators studying thin glass plates as well as 50 μm hollow glass spheres have observed that breakdown strengths change from approximately 30 kV/cm to approximately 4 kV/cm with a temperature change from 20°C to 200°C, while other investigators found no temperature dependence.[16] Results from this investigation with Gaston Power Station ash showed no temperature dependence.

The physical properties of the dust layers studied in this investigation are tabulated in Table II. The resistivities of the different particle size fractions are shown in Figure 7. The resistivities in the surface conduction region shown in this figure increased with increased particle size. Bickelhaupt[18] discusses the relationship of resistivity and particle size and surface area. For the different particle size fractions, the estimated diameter of voids in the dust layer ranged from 3 to 29 mm. The surface area per unit volume likewise changed an order of magnitude.

These results indicate that changes in the physical properties of the collected ash layer in a precipitator will influence precipitator operation by changing the ash resistivity and not by significantly changing the dielectric strength of the ash layer.

EROSION AND DUST LAYER SURFACES

The dust layer surfaces of large particles at low resistivities are eroded when current producing voltages are applied. A combination of electrostatic forces and mechanical forces due to "electric wind" scatters the dust, thins the layer and creates surface irregularities. This phenomenon is especially detrimental to close study of dust layers.

Gaston Power Station dust resistivities at ambient temperature and humidity (23°C and 1-2% H_2O by vol) are two or three orders

TABLE II

PHYSICAL PROPERTIES OF DUST LAYERS FORMED
FROM THE GASTON ASH PARTICLE SIZE FRACTIONS

Size Range of Fraction, μm	Medium Diameter, μm	Average Measured Porosity,* %	Cross sectional average area of void formed by contact of spheres,** μm^2	Diameter of circle with equivalent pore area, μm	No. of Particles,+ cm^{-3}	Surface of the particle with median diameter,++ μm^2	Surface per cm^3 of dust,+++ m^2
0-3	2.3	76.7	6.15	2.8	3.66×10^{10}	1.66×10^{1}	.608
3-7	3.6	69.9	10.6	3.7	1.232×10^{10}	4.072×10^{1}	.502
7-15	8.2	62.4	39.2	7.1	1.30×10^{9}	2.11×10^{2}	.274
15-25	14.5	57.3	98.9	11.2	2.675×10^{8}	6.60×10^{2}	.177
+25	40	54.7	676.5	29.3	1.35×10^{7}	5.03×10^{3}	.068

Determined by Bahco analysis

*Porosity = $P = 100\% \times \left(1 - \frac{\text{Apparent density of material}}{\text{True Density}}\right)$

**Cross sectional area of void formed by contact of spheres[17] = $A = .36d^2 \left[\frac{.985}{1 - \frac{P}{100}}\right]$ d = diameter based on assuming all the particles are of the same diameter.

+number of particles per unit vol. = $N = (1 - \frac{1}{100})/\sigma_v \, d^3$ $\sigma_v = \frac{\pi}{6}$ for spheres[17]

++surface area of particle = $A_s = \pi d^2$

+++surface are per cubic centimeter of dust layer = $NA_s = \pi(1 - \frac{P}{100})/\sigma_v d$, for spheres = $6(1 - \frac{P}{100})/d$

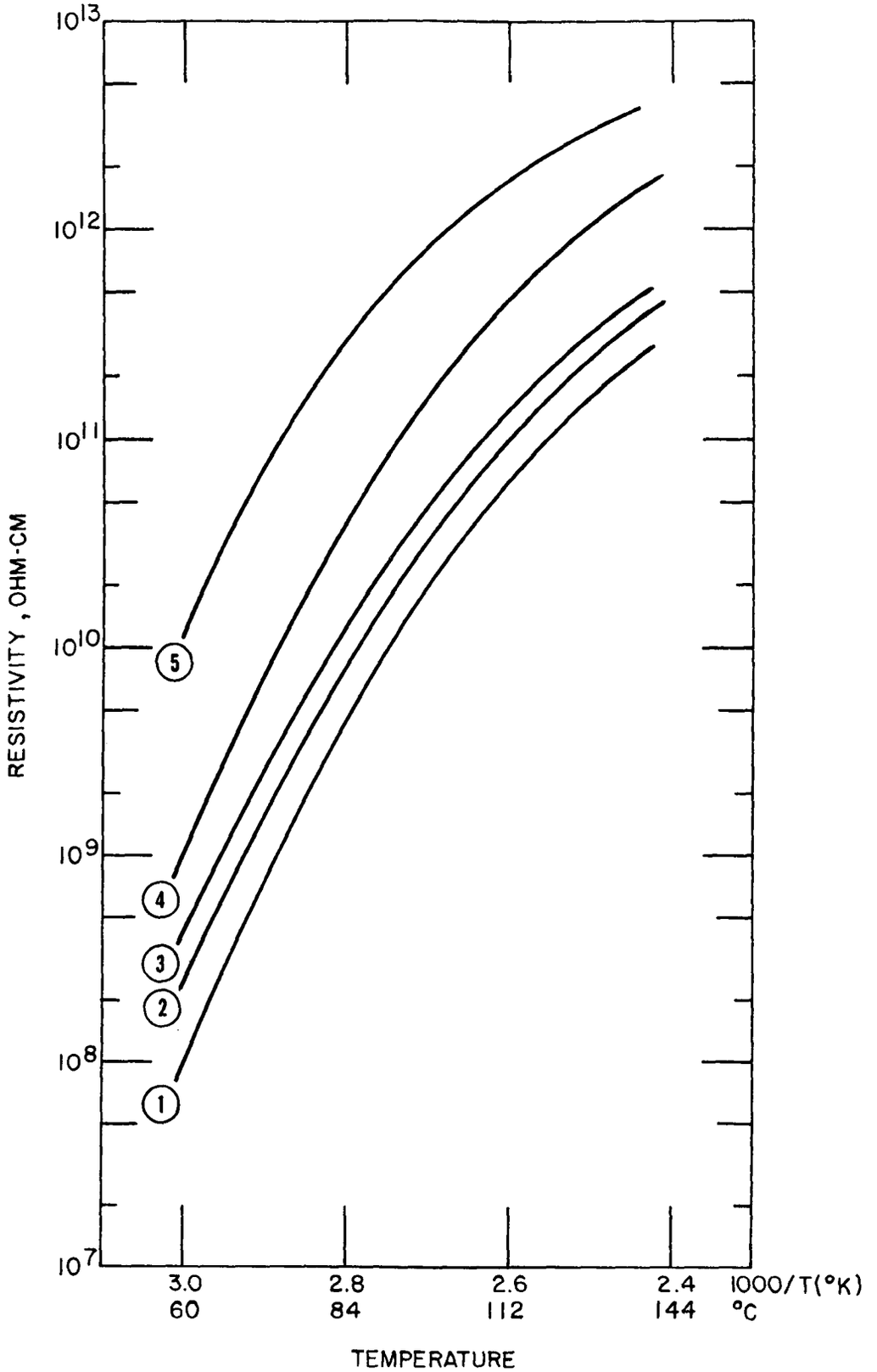

Figure 7. Resistivity vs. temperature for different particle size fractions; 1) 74.5% P(Porosity), 0-3 μm; 2) 67.8% P, 3-7 μm; 3) 64.7% P, 7-15 μm; 4) 58.0% P, 15-25 μm; 5) 54.3% P, >25 μm; 9.4% water vapor by volume.

of magnitude lower than those at higher temperatures (180°C). Lower resistivities cause correspondingly smaller voltage drops across the dust layer for a given current density. This decreases the tensile strength of the layer. The total cohesive effects of van der Waals' forces are more pronounced for smaller particles, making them more difficult to free from a surface than larger ones.

The largest particle fraction studied, with particle diameters greater than 25 microns, was blown badly under all moisture conditions studied. A 3 millimeter layer was cleared from the plate in about three minutes at room conditions with 30 kV applied. Higher temperatures and moisture contents reduced this effect; 0-3 μm and 3-7 μm size fractions were not significantly affected by corona wind under any of the conditions investigated.

Dust was first disturbed at the outer edge of the layer, particularly at corners. Higher voltages caused blowing at all points on the surface (Figure 8 upper photograph). Craters were formed at the sites of back corona and sparkover (Figure 8 lower photograph). Large particle sizes showed peculiar patterns in the dust layer at sites of back corona and spark-over. Particles appeared to be redeposited and realigned on the surface (Figure 9 upper photograph).

With a dust layer, sparkover normally occurred on the inner plates, forming craters. It often occurred at several points on the surface. In high temperature and low moisture content conditions cracks in the surface formed between plates. Sparkover and back corona tended to occur in these cracks (Figure 9 lower photograph).

Blown dust layer, large particles
> 25 μm (Temp 86°C, Moisture 12$^{V}/_{O}$)

Craters formed by sparkover to undisturbed dust layer

Figure 8. Photographs of dust surface on the wire plate corona discharge device.

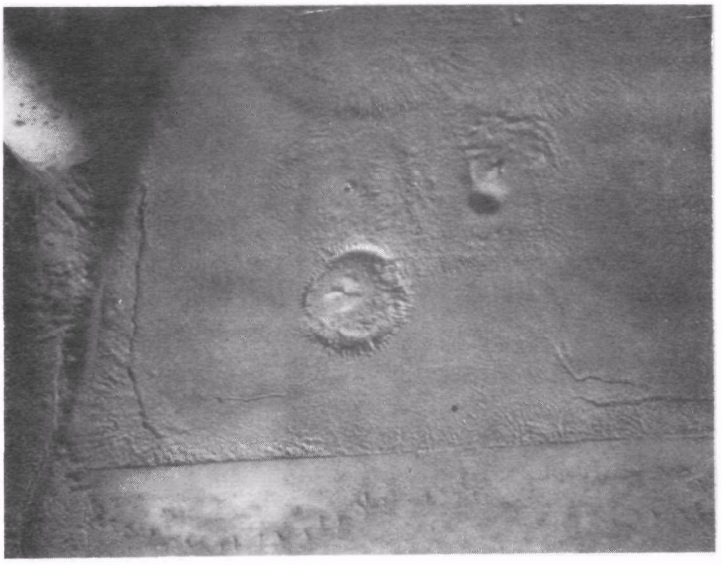

Patterns formed on dust layer composed of large particles by back-corona and sparkover

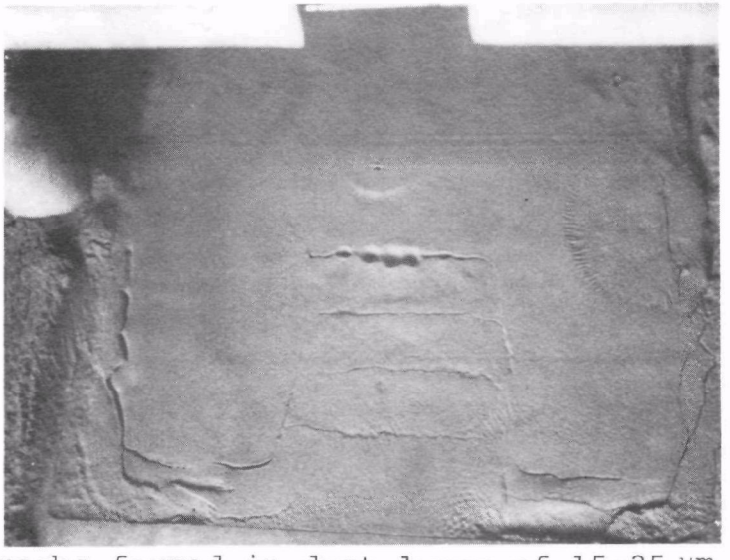

Cracks formed in dust layer of 15-25 μm particles at 180°C

Figure 9. Additional photographs of dust surfaces on the wire plate corona discharge device.

THE WIRE PLATE CORONA DISCHARGE CHARACTERISTICS

The voltage-current (V-I) characteristics for the wire-plate negative corona discharge device* discussed previously are plotted in Figure 10 for temperatures of 120°C and 60°C. The shift in the V-I characteristic with increasing temperature results from the decrease in gas density with increasing temperature. The series of graphs in Figure 11 show the changes in the voltage-current characteristics* that occur with an increase in ash resistivity from 3×10^9 Ω-cm to 1×10^{12} Ω-cm. The solid line in each of these plots is the characteristic obtained without an ash layer. The voltage-current characteristic with an ash layer is indicated by the circles. The dashed line is the clean plate characteristic shifted according to the theoretical voltage drop across the ash layer. The voltage drop is calculated using Ohm's Law, the measured resistivity, and the measured thickness of the dust layer.

$$\Delta V = j\rho l$$

ΔV = potential across the dust layer
j = current density
ρ = resistivity
l = depth of the ash layer.

The shift in the V-I characteristic with a 10^9 Ω-cm resistivity ash is shown in graph 1 of Figure 11. The difference between these two curves is masked in practice by variations in moisture, temperature, and corona wire characteristics between measurements with and without ash layers.

For a 10^{10} Ω-cm resistivity ash, the shift is several kilovolts and is easily observed as shown in graph 2 of Figure 11. The data points are near the shifted curve until back corona occurs.

---

*Center segment of the wire plate discharge device. Note that the V-I characteristics are plotted on semi-log scales. The curves have a normal appearance when plotted on linear scales.

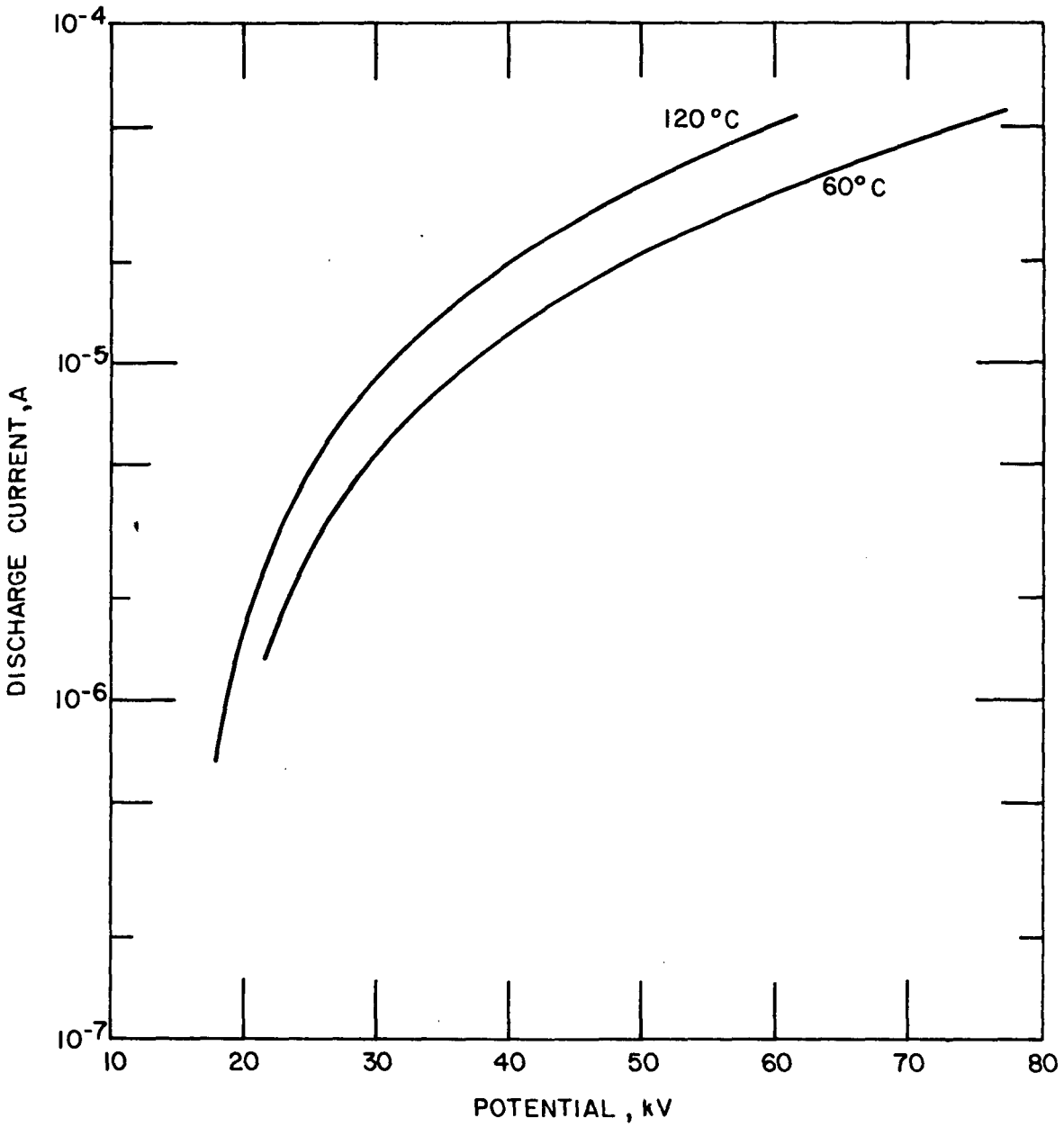

Figure 10. Clean plate voltage-current characteristics

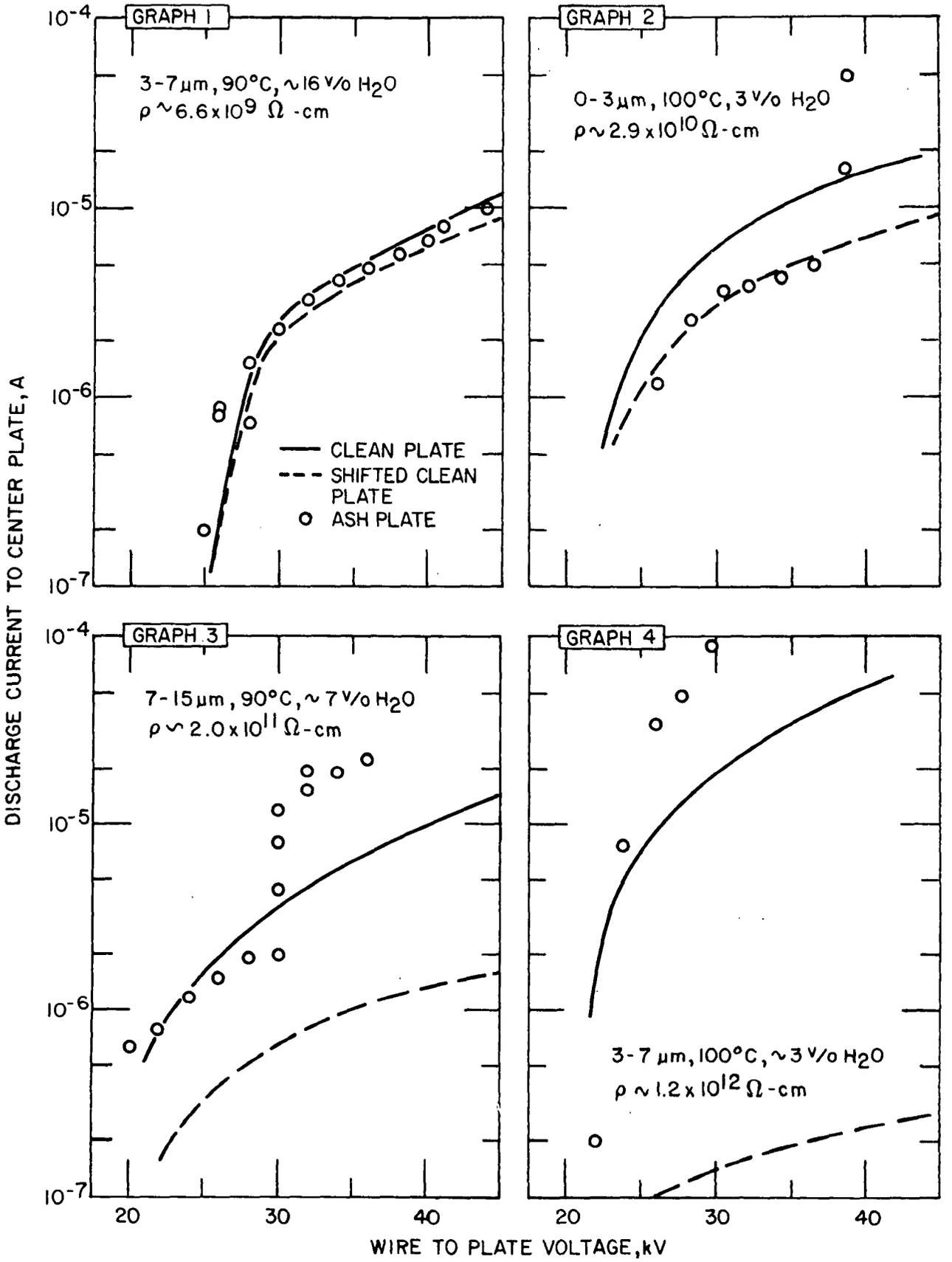

Figure 11. Voltage-current characteristics for wire plate discharge device, 3 mm dust layer.

With the formation of back corona, there is a sharp increase in current, which is clearly observed on a semi-log plot. This break in the characteristic determines the start of back corona.

For higher currents, glows were observed at various locations on the dust layer; in addition, bursts of current occurred at random intervals of approximately 0.1 to 1 msec. The burst lasted for approximately 2 μsec with peak currents of 2mA. Typical pulses are displayed in Figure 12. The individual pulses occurred less frequently than the flares observed by Penney[11] and lasted four times longer. The peak currents were a factor of 10 smaller than the 30-80 mA peak current that Penney reported. Two separate types of pulses were observed both of which occurred only when back corona spots appeared on the dust layer surfaces. The positive pulses had a high frequency component superimposed on the pulse and appear to be related to changes in the characteristics of the brushes on the corona wire. Some of the brushes appeared to change from blue to yellow when back corona formed, in agreement with an earlier observation by White.[14] The pulses indicated that the back corona spot was pulsing. These current pulses are much larger than the Trichel pulses[19] that are observed when negative corona is first initiated.

The calculated voltage drop across the dust with a resistivity of 3×10^{11} Ω-cm is indicated by the dashed curve in graph 3 of Figure 11. The measured V-I did not follow this curve. The V-I characteristics with a 10^{11} Ω-cm dust layer initially had higher currents than the clean plate characteristic and paralleled the shifted clean plate characteristic until back corona developed. Starting currents higher than clean plate starting currents were observed several times for dust layers with 10^{11} Ω-cm resistivities. A satisfactory explanation for this behavior does not exist at this time.

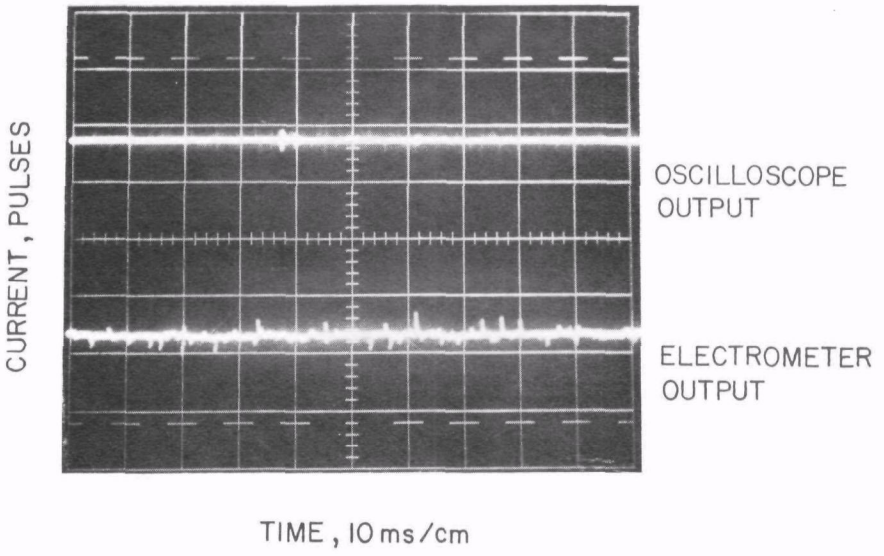

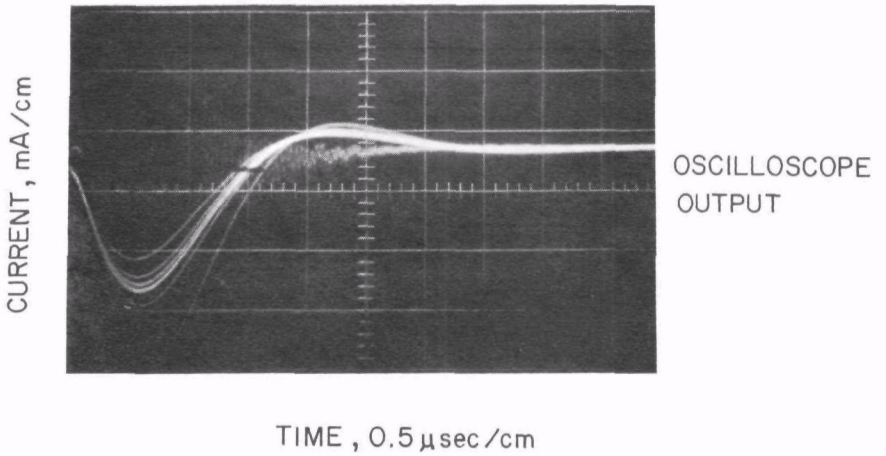

Figure 12. Oscilloscope traces of back corona pulses

In graph 4, the V-I characteristic for a 10^{12} Ω-cm ash layer is plotted. Back corona formed near the corona onset. The current increased sharply.

A comparison of the V-I characteristics of the different particle size fractions indicates that ash resistivity is the important parameter determining where back corona and where sparkover occur. The results of the measurements are shown in Table III. The fines have the highest sparkover potential and the lowest resistivity. Penney[2] also found higher sparkover voltages with his fine particle size fraction, which had higher resistivities than his larger particle sizes. However, Penney's large particle size fraction contained large carbon particles, which reduced the resistivity of the ash.

The chemical compositions of the ash fractions used in this study are tabulated in Table IV. The data indicate that the carbon content-loss on ignition (LOI) of these size fractions was largest in the small particle size fraction and least in the large particle size fraction. Measurements by Bickelhaupt[20] show that resistivity of fly ash is unaffected by a carbon content of 10% or less. Except for the carbon content, the compositions of the size fractions are similar. However, as shown by Bickelhaupt[18] the resistivity of the ash decreased with decreasing particle size in the surface conduction region.

As mentioned previously, the surface characteristics of ash layers formed from the different particle size fractions varied significantly because of the decrease in the cohesiveness of the dust with increasing particle size. The small particle size fraction produced dust layers that cracked when the Teflon base of the wire plate discharge base expanded. The large particle size fractions produced dust layers that were easily blown by the corona

TABLE III

SPARKOVER AND BACK CORONA VOLTAGES FOR FIVE DIFFERENT PARTICLE SIZE FRACTIONS

Particle Size Fraction, μm	Temperature,* °C	Moisture* Volume, %	Sparkover Voltage, kV	Back Corona Voltage, kV	Back Corona Current Density, $\mu A/cm^2$	Resistivity, Ω-cm
0-3	90	13.5	52	52	>1.7	$1x10^9$
3-7	90	11.8	48	44	.99	$1.9x10^{10}$
7-15	90	14	46	42	.76	$2.4x10^{10}$
15-25	90	12	42	42	.71	$3.6x10^{10}$
>25	90	12	42	34	.25	$1.5x10^{11}$

* Chosen to obtain reasonable resistivities.

TABLE IV

CHEMICAL ANALYSES OF SIZE FRACTIONATED FLY ASH SAMPLES

	Particle Size Range					
	0-3μ	3-7μ	7-15μ	15-25μ	+25μ	Avg.
Chemical Constituent						
Li_2O	.08	.08	.08	.08	.08	.08
Na_2O	1.16	1.07	.544	1.34	1.23	1.07
K_2O	2.86	2.63	2.63	2.67	2.67	2.69
MgO	1.13	1.08	1.17	1.21	1.28	1.17
CaO	1.59	1.84	1.54	1.41	1.50	1.58
Fe_2O_3	6.62	5.93	6.71	7.72	12.84	7.96
Al_2O_3	28.136	29.52	30.09	27.23	24.66	27.92
SiO_2	45.04	45.35	47.39	49.74	51.14	47.73
TiO_2	3.19	2.74	2.80	2.87	2.74	2.87
P_2O_5	0.705	0.482	0.321	0.356	0.496	0.47
SO_3	0.81	0.54	0.29	0.22	0.09	0.39
LOI	8.47	8.71	6.16	3.67	0.85	5.57
	98.981	99.432	99.435	98.30	99.48	99.50
	+0.81	0.54	0.29	0.22	0.09	
SUM	99.79	99.97	99.725	98.52	99.57	

wind when using conditions which produced low resistivities. Penney[2] also experienced this problem. These conditions affected our data. For example, sparking normally occurred at locations on the anode plate where a crack was present in the dust layer. However, the effects appeared to be slight compared to changes in resistivity.

The influence of ash resistivity on the formation of back corona is displayed in Figures 13 and 14. In Figure 13 the voltages at which back corona occurred and at which sparkover occurred as determined from the measured V-I characteristics are plotted as function of resistivity. The horizontal lines at the top of the graph indicate the voltages at which sparkover occurred for various temperatures and show a decrease in sparkover potential with increasing temperature. The dashed curve indicates the potential between the outer surface of the dust layer and the corona wire at the formation of back corona or sparkover for a 3 mm dust layer with a dielectric strength of 24 kV/cm. The solid curve is an estimate of the average voltage at the formation of back corona. The data points for the voltages at which back corona occurred are denoted by circles and the voltages at which sparkover occurred are denoted by triangles.

For ash with a resistivity greater than 2×10^{10} Ω-cm, the current density at sparkover is large enough that the ohmic voltage drop in the dust layer exceeds the dielectric strength of the ash layer and back corona is observed at voltages significantly below the sparkover voltage.

The dashed curve in Figure 13 was obtained by subtracting the theoretical voltage drops in the ash layer at sparkover (or at the formation of back corona if back corona existed before sparkover) from the average voltage curve for the formation of back

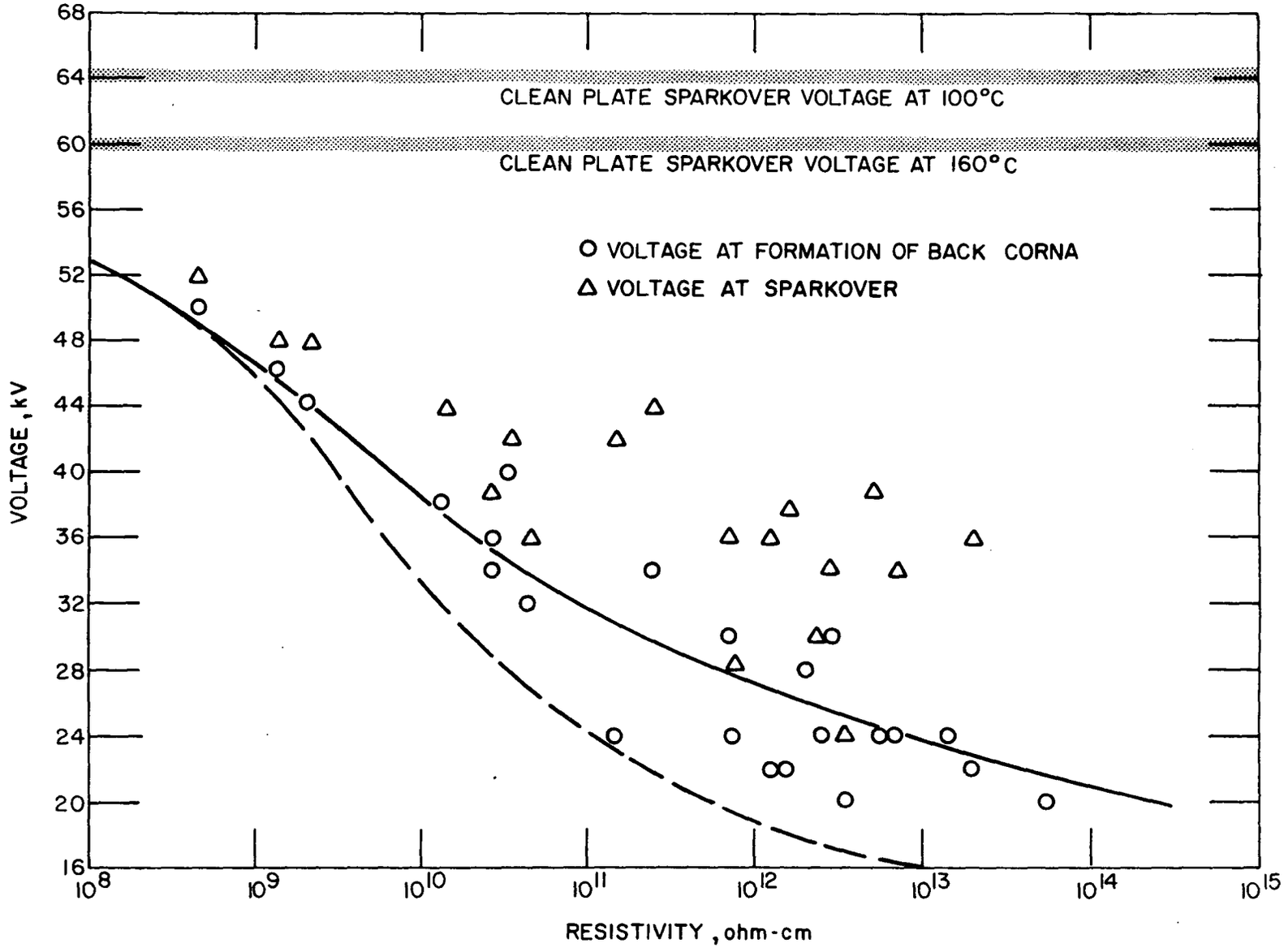

Figure 13. Wire plate corona discharge device voltages for sparkover and for formation of back corona as a function of resistivity; wire to plate spacing 6 cm. Solid curve estimate of the average voltage at formation of back corona, dashed curve potential between dust surface and wire at formation of back corona.

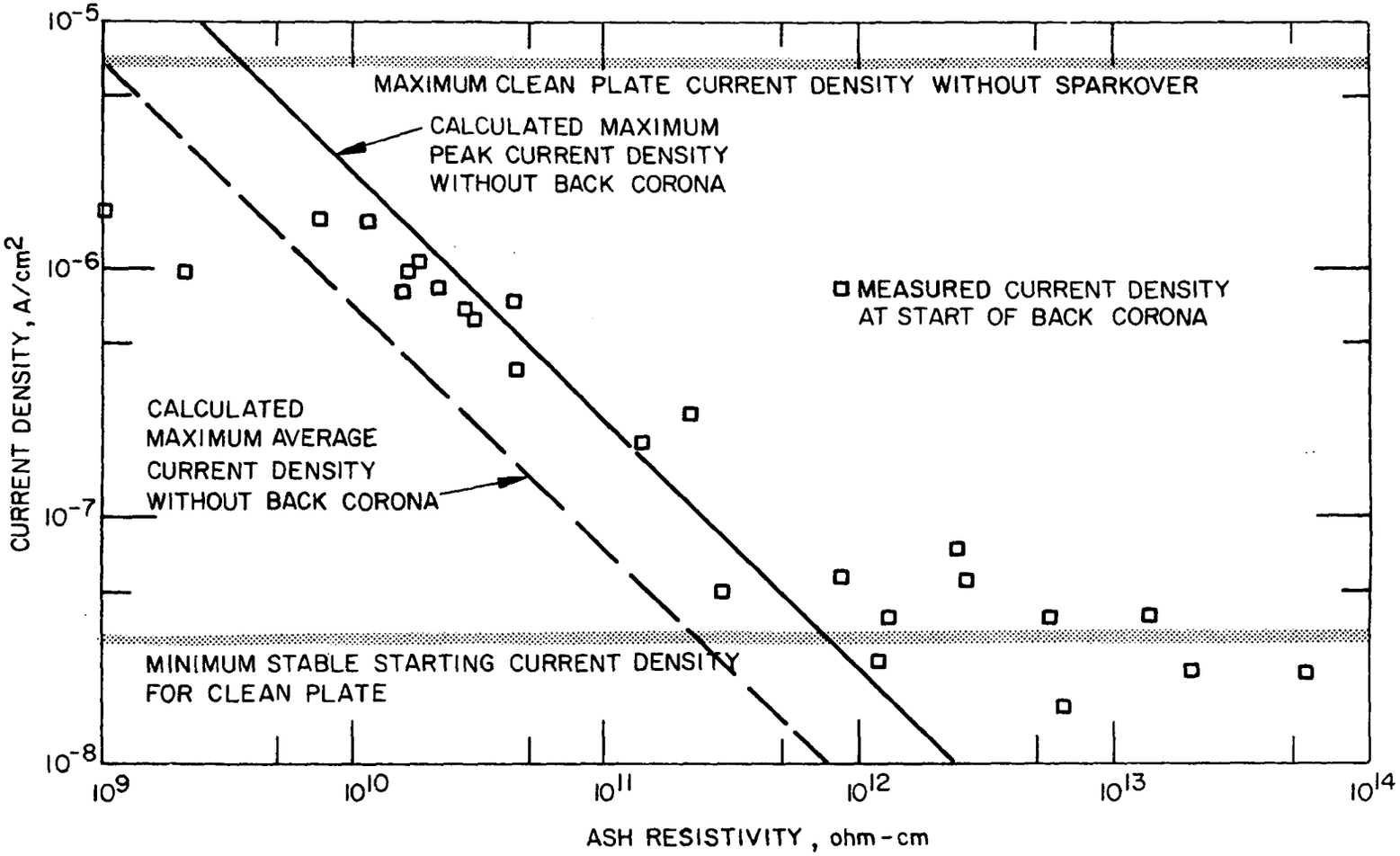

Figure 14. Current densities for formation of back corona in the wire plate corona discharge device as a function of resistivity

corona. The voltage drop across the ash layer after the formation of back corona is assumed to remain fixed at a voltage equal to the product of the layer thickness and the dielectric strength of the ash.

For ash with a resistivity below $2x10^{10}$ Ω-cm, the current density at sparkover produced voltage drops in the dust layer that were less than the measured breakdown voltage of the dust layer. However, as shown in Figure 13, the voltages at sparkover were substantially below the clean plate sparkover voltages and back corona was observed just before sparkover. A full explanation is not available. Cracks and distortions in the dust layers can produce high electric field regions that probably account for some of the reduction in sparkover voltages. The reduction in the sparkover voltage is also partially the result of the smaller spacing between the wire and dust layer when compared to the separation between the wire and plate.

In a precipitator, the voltage drop across the dust layer will vary in time as the thickness of the dust varies and, depending on the dust resistivity and operating current densities, the changing voltage drop can account for changes in precipitator performance with time, especially when a precipitator is first turned on.

Although there is considerable scatter, the data in Figure 13 show that the potential difference between sparkover and the formation of back corona increases with increasing resistivity.

Theoretically, back corona occurs when the electric field produced in the dust layer is greater than the dielectric strength of the ash. The average electric field in the dust layer is given by the product of the current density and the resistivity

of the layer. Thus, current density at the formation of back corona is given by

$$j = \frac{E_{breakdown}}{\rho \text{ at breakdown}}$$

where $E_{breakdown}$ is the dielectric strength of the dust layer and $\rho_{breakdown}$ is the resistivity of the ash layer at breakdown.

The solid diagonal line in Figure 14 is a graph of the above expression for $E_{breakdown}$ = 24 kV/cm. The two dashed horizontal lines represent the respective maximum and the minimum current densities achievable with the wire plate corona device used in this series of experiments. These horizontal lines set the operating limits for the device.

The squares in Figure 14 represent either the minimum current density obtained if back corona occurred as soon as the corona discharge was initiated or the current density at which the back corona occurred as determined from the V-I curves and back corona current pulses.

A comparison of the solid diagonal line and the squares indicates reasonable agreement between the theory of the formation of back corona as function of resistivity and the actual processes. The two data points near 10^{11} Ω-cm that lie above the diagonal line correspond to data from V-I curves similar to the one shown in graph 3 of Figure 11.

The average current density for the total plate area of the wire plate discharge device was 0.3 to 0.5 times the peak current density.

Hence, the dashed diagonal line in Figure 14 represents the maximum average current density at which the device could be operated without the formation of back corona. Likewise, the average operating current density of precipitators is below the peak theoretical predicted values.

VARIATION IN SPARKOVER VOLTAGE AS A FUNCTION OF THE WIRE TO PLATE SPACING

The current densities at which back corona developed as a function of the wire to plate spacing for the corona discharge device are displayed in Figure 15. The current densities at which sparkover occurred are indicated by squares for the clean plate. The sparkover voltages as a function of wire to plate spacing for both the clean plate and the ash covered plate are plotted in Figure 16.

The current density plot suggests that the current density for the formation of back corona is independent of the wire to plate spacing as predicted by theory. Using $E = j\rho$ to calculate the electric field in the dust layer when back corona forms, we obtain a value of 16.5 kV/cm*, which is approximately 6 kV/cm less than the measured dielectric strength of the dust layer. The estimated error in the resistivity measurement can account for the difference between this calculated dielectric strength and the measured dielectric strength.

Although changing the wire to plate spacing does not affect the current density at which back corona forms, it does decrease the voltage at which back corona and sparkover occurs as illustrated by Figure 16. The decrease in the sparkover voltage when a dust layer is present results from the increase in peak current density that is obtained for a given voltage when the wire to plate spacing is decreased. The significant increase in current density with

---

* $j = 1.1\ \mu A/cm^2$

  $\rho \simeq 1.5 \times 10^{10}\ \Omega$-cm

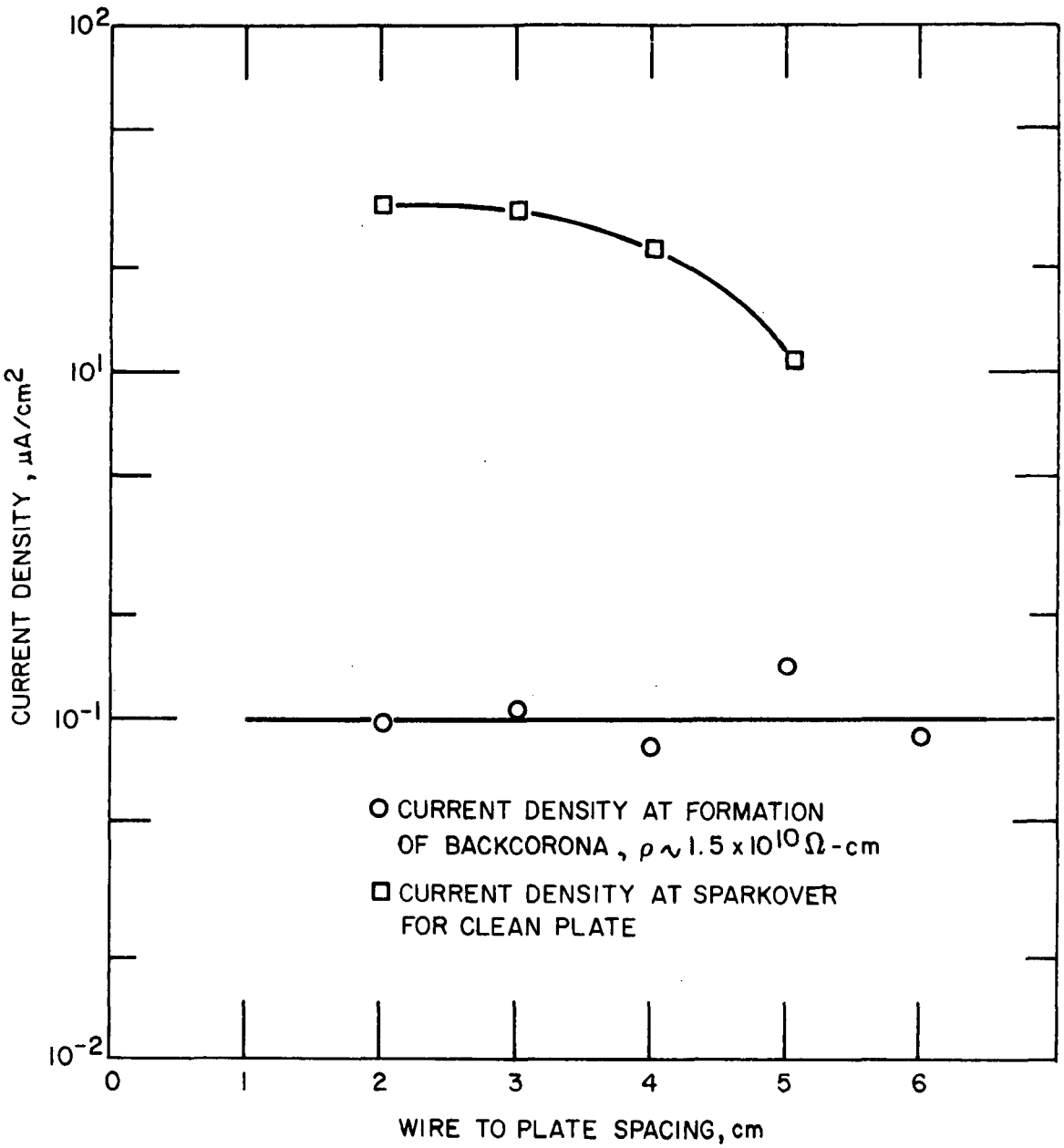

Figure 15. Current densities for sparkover and for formation of back corona as a function of wire to plate spacing.

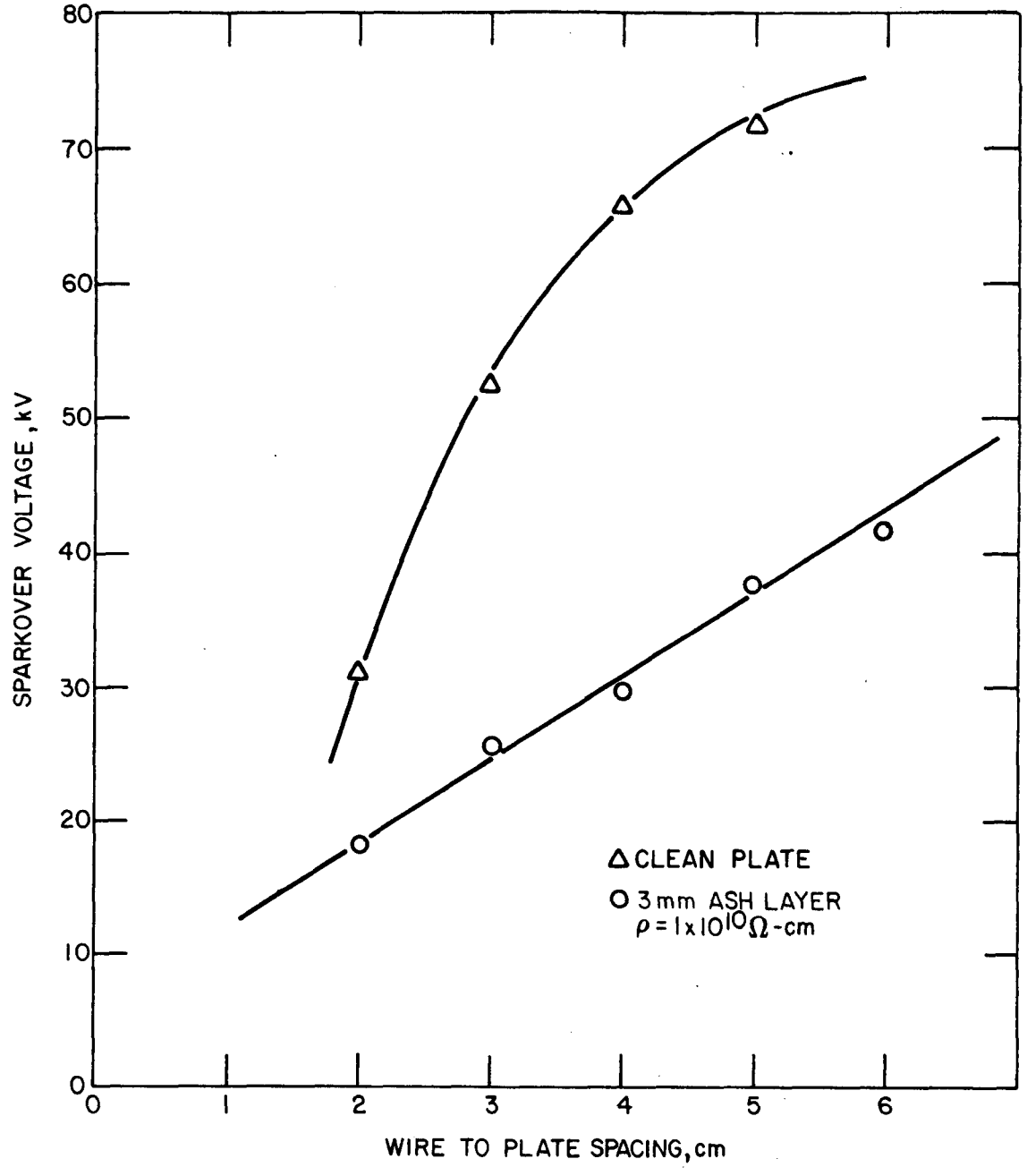

Figure 16. Sparkover voltage as a function of wire to plate spacing.

decreasing wire plate spacing is illustrated in Figure 17 by the current density distributions obtained at a wire potential of 21 kV with wire to clean plate spacings of 3 cm and 5 cm. The ratio between the peak current density and the average current density is also increased by decreasing the wire to plate spacing.

The effects discussed above can be expected to occur in full scale units where there is poor alignment of the wire and plate. Back corona will form at a lower average current density than the resistivity of the ash would indicate and the operating voltage throughout the section with poor alignment will be greatly reduced.

CURRENT DENSITY VARIATIONS

The current densities to small rectangles on the plate parallel to the corona wire are plotted in Figure 18 and 19. The solid lines in Figure 18 represent the clean plate current density distributions perpendicular to the corona wire for voltages of 22 kV, 28 kV, 40 kV, and 52 kV.

The data points represent the current density distributions for a dust layer with and without back corona. This data shows that the effect of back corona is localized in the region in which the electrical breakdown occurs. In Figure 19, current density distributions for a 6×10^{12} Ω-cm resistivity dust layer are plotted. The area covered by back corona is much larger than in the previous case. The outer two segments appear to be free of back corona.

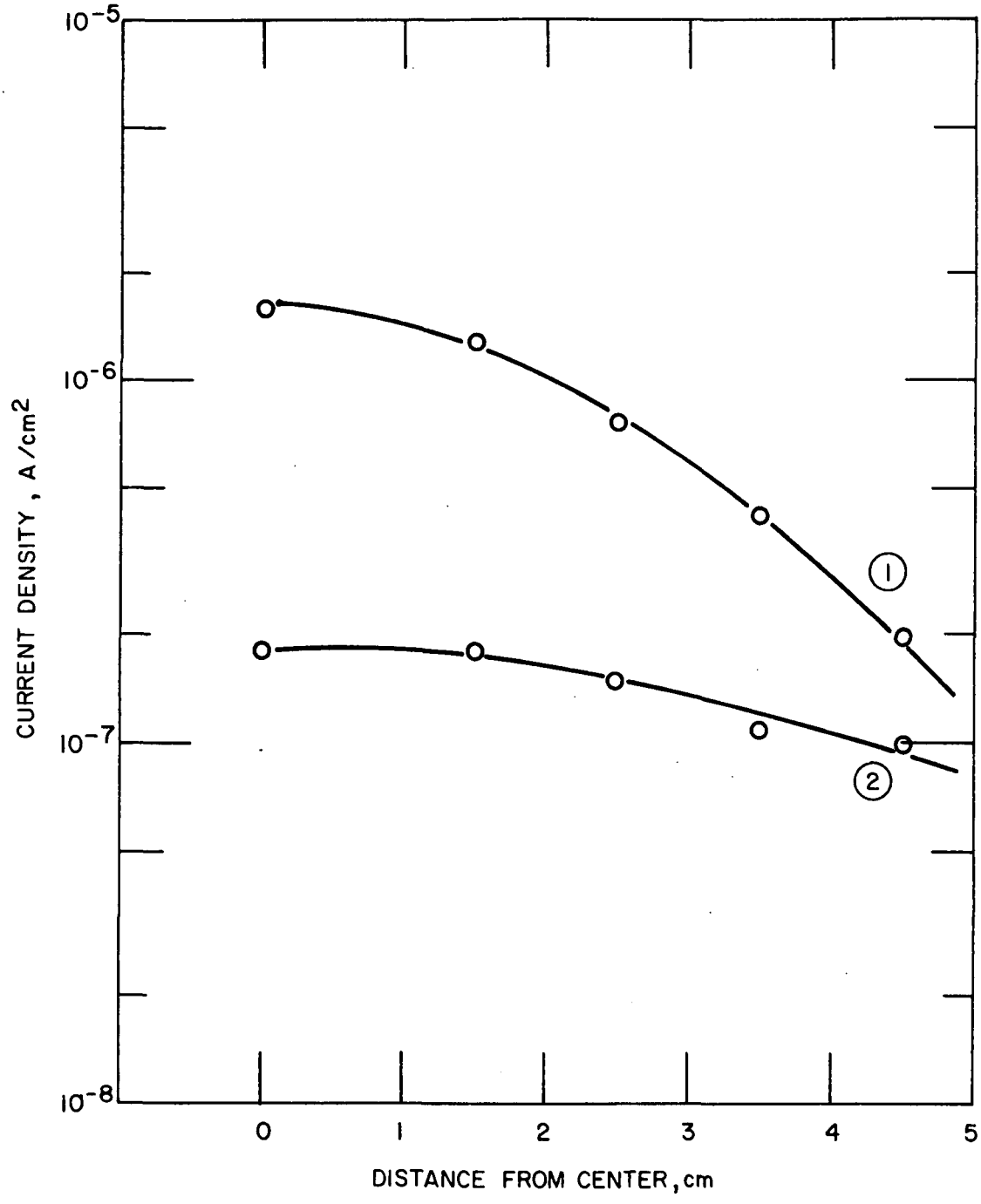

Figure 17. Current density distributions: Wire potential of 21 kV, clean plate spacings of 1) 3 cm and 2) 5 cm

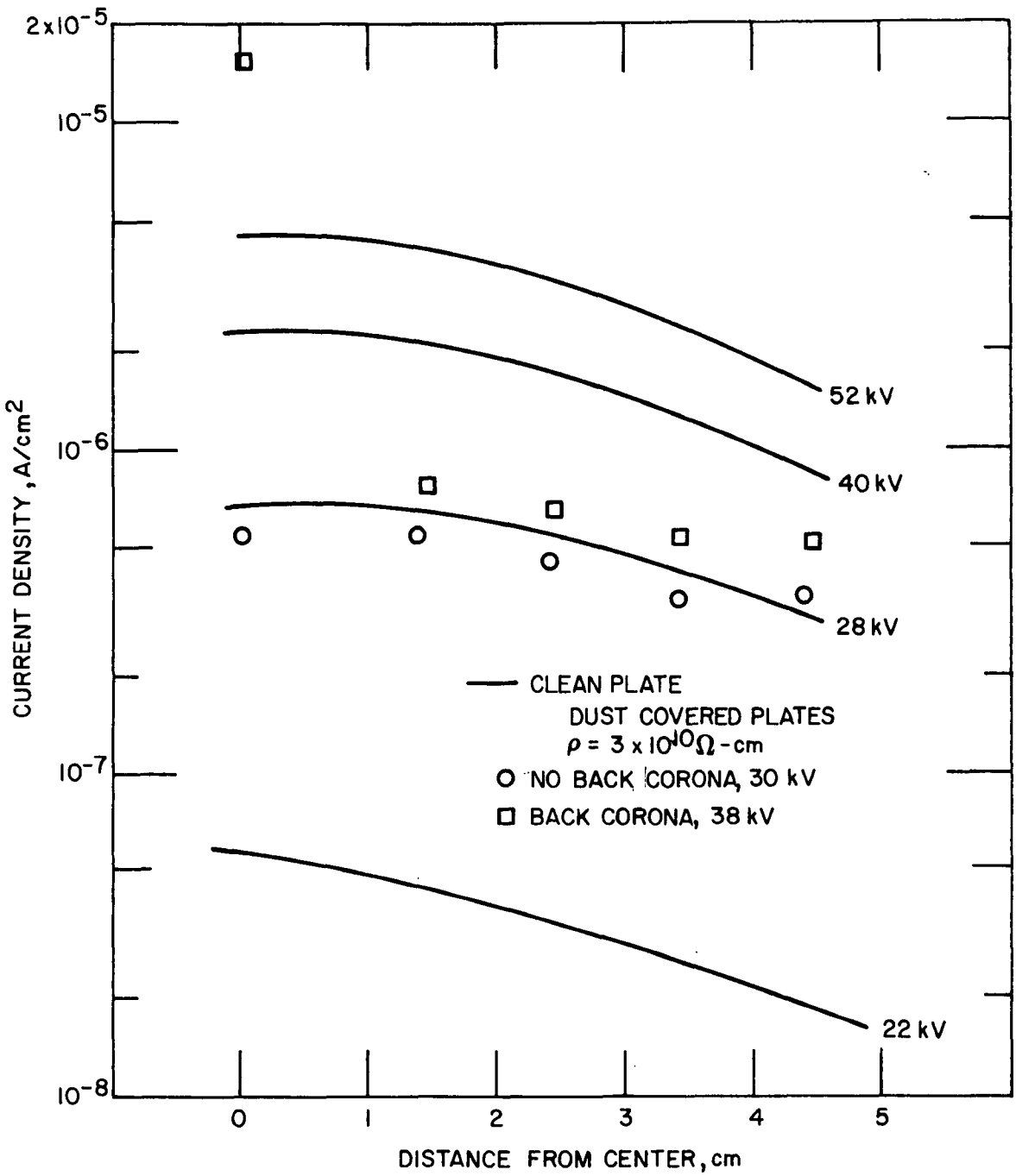

Figure 18. Current density distributions with and without back corona

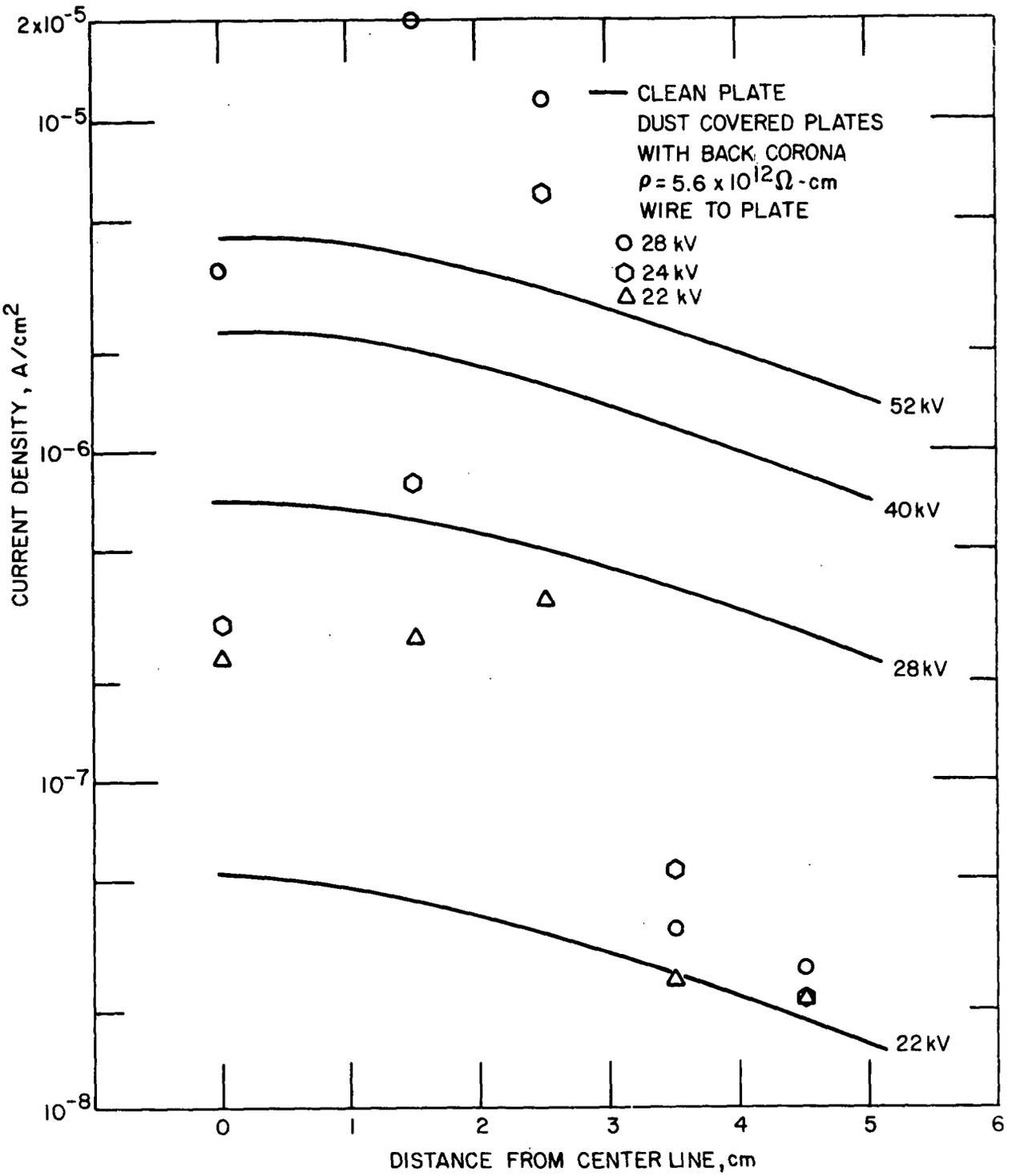

Figure 19. Current density distributions for clean plate at several applied potentials and for dust covered plate with back corona

SECTION VI

MEASUREMENTS ON FULL-SCALE PRECIPITATORS

The operating current densities versus resistivity for several full-scale precipitators are plotted in Figure 20. The resistivities were measured using a point-to-plane resistivity probe.[21] The operating current densities are the typical spatial and time average current densities that existed during efficiency tests. A large portion of the data in this plot came from an ash conditioning study by Dismukes.[1]

An analysis of the data plotted in Figure 20 is difficult for several reasons. There is no well defined point for the most efficient current density setting when sparking and back corona occur. Thus, the operating current densities are set to some degree by the operator's opinion as to what the best setting is. A second problem is that in several cases the operating current densities are set by the power or current capability of the power supply and not by the electrical characteristics of the precipitator. A third problem is that the <u>average</u> current density is plotted; and back corona and sparking depend on <u>peak</u> current densities, which vary from one unit to another. In one case, plant personnel stated that the plates had buckled and that the wire to plate spacing varied throughout the unit (data point 6). The operating average current densities were substantially below those that would normally be expected for the resistivity measured at that installation. But, when consideration is given to the effect that misalignment has on peak current densities, the observed current densities are not surprising. Another difficulty is in the variation in resistivity across the width of the precipitator when a Lundstrom preheater precedes the unit.* Laboratory measurements also suggest that variations in resistivity along the length of the precipitator may occur for temperatures at which

---

*Documentation showing the location of the resistivity measurements with respect to the precipitator sections was not available for much of the data plotted in Figure 20.

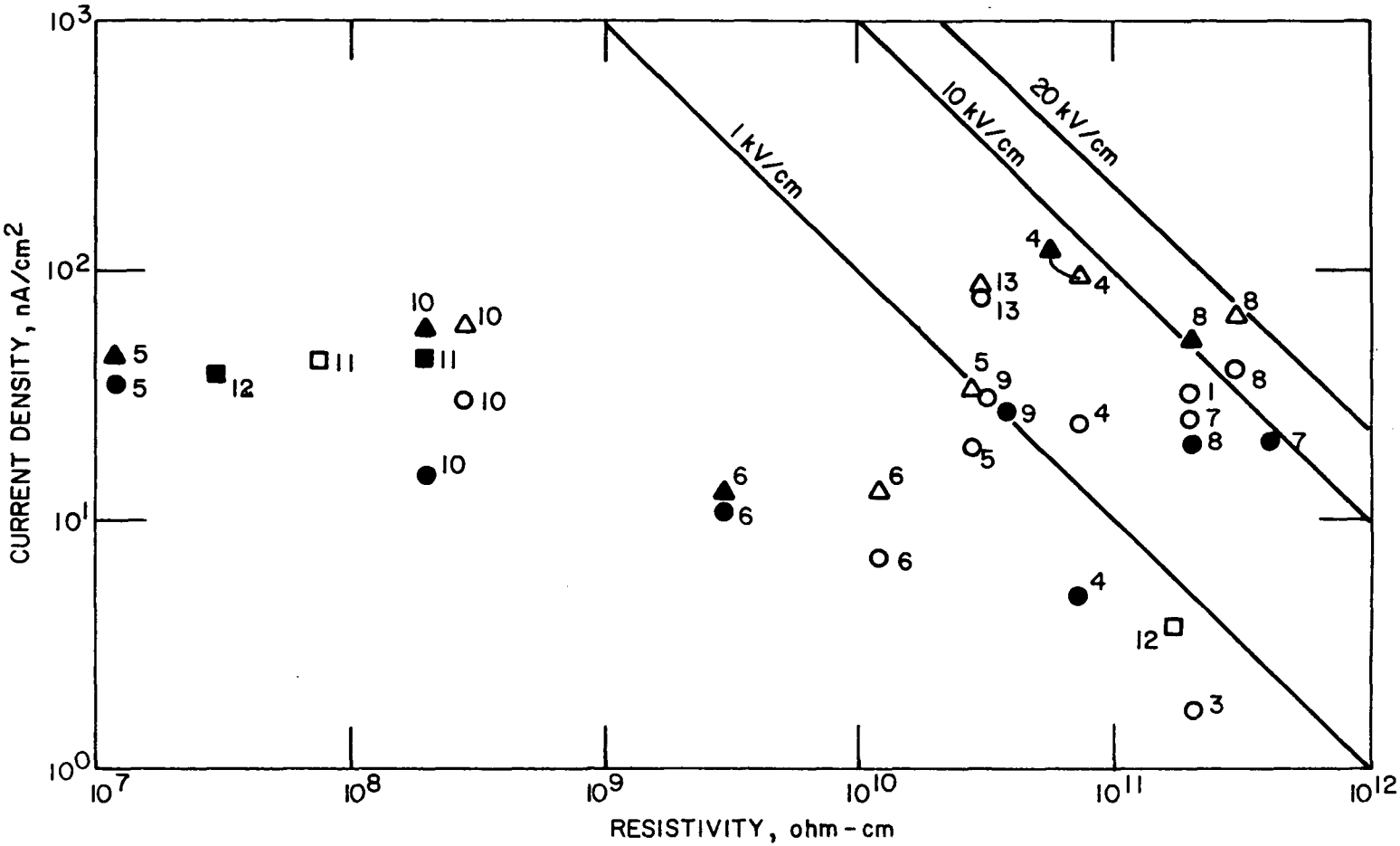

Figure 20. Operating current densities as a function of resistivity for various plants tested by Southern Research Institute. Numbers refer to data in Table V. Circles, inlet sections; triangles, outlet sections; squares, unknown sections; solid symbols, either NH_3 or SO_3 injection.

TABLE V

PRECIPITATOR ELECTRICAL DATA

Plant No.	Resistivity, Ω-cm	Electrical Section	Operating Voltage, kV	Operating Current Density, nA/cm^2	Injection	Comment
1	2×10^{11}	Inlet	40	33		All plants coal fired boilers except as noted
		Outlet	36	33		
2	5.3×10^{10}	Inlet	48	49		
		Outlet	44	33		
3	2×10^{11}	Inlet	50	2		Cement plant
		Outlet	22	25		
4	7.3×10^{10}	Inlet	40	25		
		Outlet	46	95		
	7.3×10^{10}	Inlet	41	5	NH_3	
		Outlet	44	95	NH_3	
5	2.8×10^{10}	Inlet	39	20		
		Outlet	35	33		
	1.3×10^{7}	Inlet	38	35	32 ppm SO_3	
		Outlet	36	45	32 ppm SO_3	
6	1.2×10^{10}	Inlet	24	8		Electrode misalignment
		Outlet	30	14		
	3.0×10^{9}	Inlet	30	11	14 ppm SO_3	Electrode misalignment
		Outlet	36	13	14 ppm SO_3	
7	2.0×10^{11}	Inlet	38	25		
	4.0×10^{11}	Inlet	41	22	14 ppm NH_3	
8	3.0×10^{11}	Inlet	39	40	14 ppm NH_3	
		Outlet	-	70		
	2.2×10^{11}	Inlet	42	22	13 ppm NH_3	
		Outlet	40	60	13 ppm NH_3	
9	3.0×10^{11}	Inlet	-	31		
	3.8×10^{10}	Inlet	35	29	5 ppm NH_3	
10	2.8×10^{8}	Inlet	45	30		
		Outlet	40	62		
	2.0×10^{8}	Inlet	47	15	20 ppm NH_3	
		Outlet	41	60	20 ppm NH_3	
11	2.0×10^{8}	Inlet	38	45		
		Outlet	29	45		
	8.0×10^{7}	Inlet	46	20	10 ppm NH_3	
		Outlet	30	45		
12	1.6×10^{11}	Inlet	37	4		
		Inlet	41	38		
13	3.0×10^{10}	Inlet	31	83		
		Outlet	29	95		

surface conduction is important (< 230°C).

For resistivities less than 10^9 Ω-cm, direct current densities larger than 1 μA/cm^2 are feasible without exceeding the dielectric strength of the collected dust layer. However, current densities in field units did not exceed 0.1 μA/cm^2 even for these low resistivities.

There are several reasons for this, one of which is that several of the units are equipped with power supplies that are inadequate. A second reason is the large size of field units. It is not unusual for a power supply to handle a plate area of 300 m^2 (3000 ft^2) which is much larger than the 100 cm^2 that our laboratory corona discharge device had. This increased area and the impracticality of machining rounded edges on all parts of a field unit greatly increase the probability for sparkover. Our laboratory measurements also indicated that clean plate sparkover voltage and current density are reduced to some degree even by low resistivity dust layers.

In some installations the current appeared to be limited by space charge, especially when ammonia was injected as an agent. This point is discussed by Dismukes in a recent report.[1] He suggests that NH_3 combines with SO_3 to form a fine particulate which results in a greatly increased space charge. This in turn results in increased operating voltages, decreased current densities, and increased sparkover rates. These occur without a significant increase in resistivity and show that resistivity is not the only factor that can increase sparkover rates. Calculations of the effects of particle space charge for cylindrical corona indicate that the space charge results in a higher electric field at the passive electrode.[22] For negative corona, the field strengths at the anode would be increased and this could lead to

lower sparkover potentials than those obtained without a dust loading.

A comparison of the inlet and outlet data shown in Figure 20 indicates that in most cases the outlet current density exceeds the inlet current density, while the inlet voltage exceeds the outlet voltage. There are two possible explanations for the variations in the voltage-current characteristics from the inlet to outlet. One attributes the variations to changes in dust loading and the other to changes in the thickness and resistivity of the collected dust layer.

The effect of a variation in resistivity from the inlet to the outlet is illustrated by the following considerations. If a resistivity of 10^{11} Ω-cm is obtained in the inlet and 5×10^{10} Ω-cm in the outlet, the inlet peak current density could be as high as 200 nA/cm^2 without back corona and the outlet could be as high as 400 nA/cm^2 for a breakdown strength of 20 kV/cm.

A half order of magnitude change in the resistivity of the collected dust layer from the inlet section to the outlet section of a precipitator is reasonable. Our laboratory measurements show a decrease in ash resistivity of nearly one order of magnitude for particle size fractions with mass median diameters of 40 to 2.3 μm. The resistivity decreases with decreased particle size for temperatures at which surface conduction is important. Thus, a decrease in resistivity from the inlet section to the outlet section results from the fractionation of the ash into a larger particle size fraction in the inlet section and smaller particle size fractions throughout the rest of the unit. In addition, a change in resistivity can result from a temperature variation from the inlet to the outlet. For hot precipitators, the resistivity would be expected to increase from inlet to outlet and for cold precipitators, the resistivity would decrease from the inlet to outlet.

Average current densities depend on the spatial variation and time variation of the current. For full wave rectification and no filtering, the time average current density is 70.7% of the peak current. Typical spatial variations result in spatial average currents equal to 60% of the peak currents.

Thus, the time and spatial average current equals approximately 50% of the peak current. For our hypothetical problem, the maximum possible average currents without back corona are estimated to be 100 nA/cm^2 for the inlet and 200 nA/cm^2 for the outlet. If the depth of the collected dust layer is the same in the inlet and outlet, for the above conditions, the voltage drop across the dust layers is the same in both sections. For the same configuration in both sections, the operating voltage across the discharge should be higher in the outlet since the currents are higher. However, this does not agree with most of the data tabulated in Table V. Theoretically, the thickness of the dust layer decreases exponentially throughout the precipitator if rapping variations are neglected. This results in larger voltage drops across the inlet dust layers when both units are operated with current densities near the critical value for the electrical breakdown of the dust layer. This can lead to higher voltages in the inlet sections than in the outlet sections.

The above explanation for the variations in electrical characteristics from the inlet to the outlet is unsatisfactory for low resistivities ($<5 \times 10^9$ Ω-cm), where voltage drops less than 250 V occur for 0.5 cm thick dust layers and a current density of 0.1 $\mu A/cm^2$. The decrease in the space charge produced by the charged suspended particulate from the inlet sections to the outlet sections appears to be the dominant reason for larger currents and lower voltages in the outlet sections.

The time required for changes in the voltage-current characteristics gives some indication of the importance of the above mechanism. Dismukes[1] observed that when ammonia was injected the time lag between injection and the effect on precipitator operation was very short. In contrast, resistivity effects take longer to occur, since they depend on the accumulation of dust on the collecting plates.

REFERENCES

1. Dismukes, E. B. Conditioning of Fly Ash with Ammonia. In: Proceedings, Symposium on Electrostatic Precipitators for the Control of Fine Particles. Pensacola Beach. Environmental Protection Agency, Washington, D. C. Publication Number EPA-650/2-75-016. January, 1975. NTIS PB 240440/8WP. p. 257-287.

2. Kercher, H. Electric Wind, Back Discharge and Dust Resistance as Parameters in Electrostatic Precipitators. Staub-Reinhalt. Luft (in English). 29(8): 14-20, 1969.

3. Penney, G. W., and T. E. Alverson. Influence of Mechanical Collection on Electrostatic Precipitator Sparkover Voltage—A Laboratory Simulation. IEEE Trans. Ind. Gen. Appl. 7(3): 433-438, May-June, 1971.

4. Wolcott, E. R. Effects of Dielectrics on the Sparking Voltage. Phys. Rev. 12:284-292, 1918.

5. Franck, S. Funkenentladungen in Luft-Staubgemischen [Spark Discharges in Air Dust Mixtures]. Z. Phys. (Berlin). 87:323-229, 1933.

6. White, H. J. Characteristics and Fundamentals of the 'Back Corona' Discharge. (Presented at Gas Discharge Conference, Brookhaven National Laboratory, Upton, N. Y., 1948.)

7. Penney, G. W. Electrostatic Precipitation of High-Resistivity Dust. Trans. Am. Inst. Electr. Eng., Part 2. 70:1192-1196, 1951.

8. Penney, G. W., and J. G. Hewitt. Some Measurements of Abnormal Corona. Trans. Am. Inst. Electr. Eng., Part 1. 77:319-327, July, 1958.

9. Penney, G. W., and S. E. Craig. Sparkover as Influenced by Surface Conditions in D-C Corona. Trans. Am. Inst. Electr. Eng., Part 1. 79:112-118, May. 1960.

10. Penney, G. W., and S. Craig. Pulse Discharges Preceding Sparkover at Low Voltage Gradients. Trans. Am. Inst. Electr. Eng., Part 1. 80:156-162, May. 1961.

11. Simm, W. Untersuchungen über des Rücksprühen bei der elektrischen Staubabscheidung. [Studies of the Back Spray in Electrical Dust Removal] Chem. Ing. Tech. (Weinheim). 3:43-49, 1959.

12. Herceg, Z., and R. M. Huey. Model for Corona Modes in Point-to-Plane Device with Coated Electrodes. Proc. Inst. Electr. Eng. (London). 120:394-399, 1973.

13. Hall, H. J. Trends in Electrical Precipitation of Electrostatic Precipitators. In: Proceedings of Electrostatic Precipitator Symposium, Birmingham, Alabama. February 23-25, 1971. p. 75-116.

14. White, H. J. Industrial Electrostatic Precipitation. Reading, Massachusetts, Addison-Wesley, 1963. p. 327.

15. Alston, L. L. High Voltage Technology, Oxford University Press, London, 1968. p. 48.

16. Morey, George W. The Properties of Glass. 2nd Edition. Reinhold Publishing Corp., New York, 1954. p. 532.

17. Dallavalle, J. M. Micromeritics. 2nd Edition. Pitman Publishing Corp., New York, 1948. p. 131.

18. Bickelhaupt, R. E. Surface Resistivity and the Chemical Composition of Fly Ash. J. Air Pollut. Contr. Assoc. 25:148-152, February, 1975.

19. Loeb, L. B. Fundamental Processes of Electrical Discharges in Gases. John Wiley and Sons, Inc., New York, 1939. p. 517.

20. Bickelhaupt, R. E. Personal Communication.

21. Nichols, G. B. and H. W. Spencer. Test Methods and Apparatus for Conducting Resistivity Measurements. Southern Research Institute, Birmingham, Alabama, Contract No. 68-02-1083. Environmental Protection Agency, Research Triangle Park, N.C., 1975.

22. Lowe, H. J. and D. H. Lucas. The Physics of Electrostatic Precipitation. Brit. J. Appl. Physics, (London), Suppl. 2:540-47, 1953.

TECHNICAL REPORT DATA *(Please read Instructions on the reverse before completing)*		
1. REPORT NO. EPA-600/2-76-144	2.	3. RECIPIENT'S ACCESSION NO.
4. TITLE AND SUBTITLE Electrostatic Precipitators: Relationship Between Resistivity, Particle Size, and Sparkover		5. REPORT DATE May 1976 6. PERFORMING ORGANIZATION CODE
7. AUTHOR(S) Herbert W. Spencer, III		8. PERFORMING ORGANIZATION REPORT NO. SORI-EAS-75-629 3134-XVI
9. PERFORMING ORGANIZATION NAME AND ADDRESS Southern Research Institute 2000 Ninth Avenue South Birmingham, Alabama 35205		10. PROGRAM ELEMENT NO. 1AB012; ROAP 21ADL-027 11. CONTRACT/GRANT NO. 68-02-1303
12. SPONSORING AGENCY NAME AND ADDRESS EPA, Office of Research and Development Industrial Environmental Research Laboratory Research Triangle Park, NC 27711		13. TYPE OF REPORT AND PERIOD COVERED Final; 4/74-12/75 14. SPONSORING AGENCY CODE EPA-ORD
15. SUPPLEMENTARY NOTES IERL-RTP Project Officer for this report is L.E. Sparks, Mail Drop 61, Ext 2925.		

16. ABSTRACT The report gives results of a study of the relationships of the electrical resistivity of fly ash, its particle size, the occurrence of back corona and sparkover, and the electrical characteristics of electrostatic precipitators (ESP's). The study included laboratory measurement of the dielectric strengths and resistivity of five particle-size fractions of a fly ash sample and measurement of the current densities and voltages at which back corona and sparkover occurred for a 3-mm dust layer covering the plate of a wire-plate negative-corona discharge device. Results showed that the peak current density for the formation of back corona depended on the resistivity of the dust covering the positive electrode. Operating current densities for full-scale ESP's are discussed in relation to fly ash resistivity.

17. KEY WORDS AND DOCUMENT ANALYSIS			
a. DESCRIPTORS		b. IDENTIFIERS/OPEN ENDED TERMS	c. COSATI Field/Group
Air Pollution	Electric Corona	Air Pollution Control	13B
Electrostatic Precipitators	Dust	Stationary Sources	11G
Fly Ash	Electric Sparks	Back Corona	
Electrical Resistivity	Flashover	Particulate	21B
Measurement			20C
			14B
18. DISTRIBUTION STATEMENT Unlimited		19. SECURITY CLASS *(This Report)* Unclassified	21. NO. OF PAGES 68
		20. SECURITY CLASS *(This page)* Unclassified	22. PRICE

EPA Form 2220-1 (9-73)